

DFT-s-OFDM-based On-Off Keying for Low-Power Wake-Up Signal

Renaud-Alexandre Pitaval and Xiaolei Tie

Abstract—5G-Advanced and likely 6G will support a new low-power wake-up signal (LP-WUS) enabling low-power devices, equipped with a complementary ultra low-power receiver to monitor wireless traffic, to completely switch off their main radio. This orthogonal frequency-division multiplexed (OFDM) signal will emulate an on-off keying (OOK) modulation to enable very low-energy envelope detection at the receiver. Higher rate LP-WUS, containing multiple OOK symbols within single OFDM symbol, will be generated using the time-domain pulse multiplexing of discrete Fourier transform spread (DFT-s-) OFDM. In this context, this paper presents a general signal design framework for DFT-s-OFDM-based OOK generation. General properties of subcarrier coefficients are derived demonstrating that only DFT of the bits needs to be computed online and repeated over the band before applying appropriate frequency-domain processing. The conventional approach of generating rectangular-like OOK waveforms is then addressed by a combination of pre-DFT bit-spreading and post-DFT processing; and the least-squares (LS) method from Mazloum and Edfors, proposed for 5G LP-WUS and also Ambient-IoT, is shown to be implementable as such. Even though aesthetically pleasing and of independent interest, rectangular-like OOK waveforms are not optimal for 5G LP-WUS scenarios due to their limited robustness to channel frequency-selectivity and timing offset, and so shaping methods for spreading the OOK spectrum and concentrating the OOK symbol energy are described and shown to improve the bit error rate performance under practical conditions.

Index Terms—OOK, DFT-s-OFDM, wake-up signal, Ambient-IoT, 5G-Advanced, 6G.

I. INTRODUCTION

The Internet-Of-Things (IoT), consisting of low-power devices, is generating renewed interest in easily decodable modulation schemes such as on-off keying (OOK). The concept of a wake-up signal (WUS) has been introduced in several standards within the wireless industry. The goal is to enable devices to significantly reduce their functionality, and thus their power consumption, until incoming traffic is indicated by the network.

In 4G LTE-M and NB-IoT technologies, 3GPP already defined a WUS to enable receiver sleep modes [1], but its reception relies on a standard OFDM radio, which still demands precise synchronization and high-precision analog-to-digital conversion (ADC). Recently, 3GPP RAN1 completed a study [2] on a so-called low-power WUS (LP-WUS), which is currently under specification for 5G-Advanced. Recent works motivated by this study can be found in [3]–[7]. Significantly larger power-saving gains [8] are envisioned if the main radio (MR) of a device could be completely switched off when no

message is coming, and being triggered only when necessary. To enable this, the device would need to be equipped with an additional lower-power radio (LR) that monitors possible incoming traffic indicated by an LP-WUS. To achieve ultra low-power consumption, the LR could employ a simple non-coherent envelope detector, through which an LP-WUS can convey information using OOK modulation. Meanwhile, at the transmitter side, an OFDM generation of the LP-WUS is preferred to facilitate implementation and multiplexing with concurrent transmissions. The design of LP-WUS signals is paving the way for other OFDM-based OOK-modulated signals considered in the 5G Ambient-IoT study [9] and likely upcoming 6G IoT technologies.

The problem of generating an OOK-modulated WUS while reusing an existing OFDM implementation has already been considered in the IEEE 802.11ba standard to ease WUS adoption. The IEEE 802.11ba WUS supports a low-rate OOK mode matching the OFDM symbol rate and a high-rate mode, doubling the rate through time-blanking within OFDM symbols. The latter, however, is non-orthogonal to concurrent OFDM signals, leading to inter-carrier interference (ICI). In the context of Wi-Fi, alternative non-orthogonal WUS designs have been proposed in [10], [11], and orthogonal designs in [12]–[14]. In [12], an OFDM-based OOK WUS is obtained from numerically-found subcarrier coefficients through minimizing a least-squares (LS) problem with constraints on ON/OFF power levels along with a zero direct current (DC) subcarrier as in legacy Wi-Fi signal format. In the work of Mazloum and Edfors [14], a more general solution is provided by deriving a precoder that maps spread bits to subcarrier coefficients such that it minimizes the LS error from a perfectly rectangular OOK signal. This LS method was one of the main preliminary approaches considered in 3GPP LP-WUS study [15], and is also considered for evaluation purposes in the ongoing 3GPP study on Ambient-IoT [9].

In this paper, we study both the time-domain (TD) and frequency-domain (FD) characteristics of DFT-s-OFDM based OOK modulation, which can enable larger OOK rate than the OFDM symbol rate by exploiting its inherent TD multiplexing property. We are primarily motivated by 5G LP-WUS application in the context of 3GPP standardization, but the provided results are general and may be of independent interest for other applications. The considered system model encompasses an overlaid bit-spreading sequence prior to DFT-precoding followed by spectrum extension (SE) and FD spectral shaping (FDSS). The bit-spreading sequence modulates the DFT-s-OFDM pulses, while SE with FDSS enables control on the number and shape of these pulses [16]. In 3GPP LP-WUS study, defining direct FD subcarrier sequences was considered

Renaud-Alexandre Pitaval is with Huawei Technologies Sweden AB, Kista 164 94, Sweden (e-mail: renaud.alexandre.pitaval@huawei.com). Xiaolei Tie is with HiSilicon, Shanghai, China (e-mail: tiexiaolei@hisilicon.com).

as an alternative to DFT-s-OFDM with bit-spreading. We link these two methods by showing that a common overlaid sequence on ON-symbols can equivalently be implemented as an FD overlaid sequence. This provides an equivalent low-complexity implementation where the DFT precoder size needs only to match the number of bits – i.e., without bit spreading. Moreover, compact DFT formulas and tables absorbing Manchester encoding are obtained for efficient storage.

Next, we focus on creating rectangular-like OOK waveforms, as considered in IEEE 802.11ba WUS and the early stages of the 3GPP LP-WUS study. We employ a linear phase ramp as the bit-spreading sequence that minimize the coherent combining of consecutive DFT-s-OFDM pulses, thereby flattening the envelope of ON symbols. We also discuss rectangular-like OOK waveforms with the additional feature of a zero DC component. Furthermore, we show that the waveform resulting from ‘LS precoding’ of [14], treated in [15] as an alternative to DFT precoding, can be obtained as a specific implementation of DFT-s-OFDM-based OOK.

Rectangular-like OOK waveforms, which may be relevant to small indoor coverage scenarios like in WiFi and Ambient-IoT, are not suitable for 5G LP-WUS. Large cell coverage, as supported in 3GPP standards, involves broader bandwidth usage, making it prone to greater frequency-selectivity and channel time dispersion. Additionally, 3GPP considered a significantly higher sampling rate at LR compared to the transmitted OOK symbol rate. In this context, as long as the OOK signal achieves a sufficient ON/OFF energy split, envelope fluctuations actually matter little. Relaxing the rectangular waveform target, shaped OOK providing improved detection performance are discussed. We formalize the effect of phase scrambling in the overlaid sequence on the power spectrum distribution, as considered in [15] to flatten the spectrum. Additionally, robustness to timing errors is achieved by concentrating energy within the ON symbols. Finally, simulation results are provided to confirm the benefits of such shaping over rectangular OOK.

The remainder of the paper is as follows. Section II introduces the LP-WUS system model from an OFDM transmitter to an envelope detector at the LR. Section III describes the OOK signal generation framework based on DFT-s-OFDM modulation highlighting its general TD and FD properties. Section IV addresses the generation of rectangular-like OOK waveform, while Section V discussed shaping methods relevant for mitigating wireless channel impairments. Numerical evaluations are presented in Section VI, and conclusions are drawn in Section VII.

II. LP-WUS SYSTEM MODEL

We consider an OOK-modulated LP-WUS multiplexed along other data using a conventional OFDM transmitter, thus enabling concurrent transmission without interference.

A. OFDM Modulation

The LP-WUS is generated by populating N_{sc} subcarriers within other data symbols, all multiplexed by an OFDM modulation using an N_{fft} -point IFFT followed by cyclic prefix

(CP) addition. While such setup avoid interference from the OOK WUS to concurrent data received by OFDM terminals, the WUS itself is intended for a non-OFDM, envelope detector based, receiver for which concurrent data may interfere and thus some guard bands may still be necessary. The total LP-WUS bandwidth allocation is thus $(N_{sc} + 2N_{GB})$ where N_{GB} are null subcarriers on each band side.

Formally, the transmitted baseband OFDM signal $s[n]$ is a superposition of the WUS $s^W[n]$ and concurrent data signal $s^D[n]$ where one CP-OFDM symbol with sample indices $-N_{cp} \leq n \leq N_{fft} - 1$ can be expressed as

$$s[n] = \sum_{k=0}^{N_{fft}-1} X[k] e^{j \frac{2\pi}{N_{fft}} nk} = s^W[n] + s^D[n] \quad (1)$$

and the LP-WUS is

$$s^W[n] = e^{j \frac{2\pi}{N_{fft}} n f_0} \sum_{k=0}^{N_{sc}-1} X^W[k] e^{j \frac{2\pi}{N_{fft}} nk}, \quad (2)$$

i.e. it is the N_{fft} -point inverse DFT (IDFT), typically implemented as a fast Fourier Transform (FFT), of the N_{sc} WUS subcarrier coefficients $\{X^W[k]\}_{k=0}^{N_{sc}-1} = \{X[k]\}_{k=f_0}^{f_0+N_{sc}-1}$ allocated at the subcarrier indices $\{f_0, \dots, f_0 + N_{sc} - 1\}$.

The LP-WUS is a complex signal where information is conveyed through the fluctuation of the envelope’s amplitude; thus its starting subcarrier index f_0 is irrelevant from signal design perspective as it only changes its global phase. For convenience, we will assume $f_0 = 0$ in analytical derivations. The value of N_{sc} will often be assumed even for simplicity and practical relevance. For numerical evaluation and illustration, $N_{fft} = 512$ will be used.

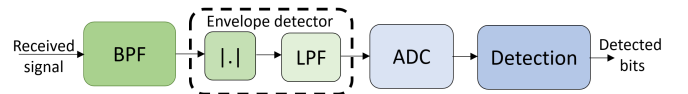


Fig. 1. A low-power wake-up receiver (LR) based on envelope detection

B. Envelope Detection

The signal arrives at the receiver via a wireless channel composed of L_p paths assumed with Rayleigh-faded attenuation $h_p \sim \mathcal{CN}(0, E_p)$ as

$$y[n] = \sum_{p=0}^{L_p-1} h_p s[n-p] + z[n] \quad (3)$$

where $z[n]$ is a zero-mean complex additive white Gaussian noise (AWGN) with variance N_0 .

We consider a LR as shown in Fig. 1. The received analog signal is first passed through a bandpass filter (BPF) centered around the LP-WUS band to remove adjacent channels; followed by an envelope detector which consists of a norm operator followed by a low-pass filter to smooth the signal, and then an ADC to finally perform detection. We will assume a Manchester encoded OOK signal, so detection can be performed by directly comparing the energy between two consecutive OOK symbols.

The receiver is considered to capture the WUS and noise power over the WUS bandwidth, including guard bands, such that the SNR is defined as $\text{snr} = \frac{E_h P_W}{(N_{\text{sc}} + N_{\text{GB}}) N_0}$ where $E_h = \sum_{p=0}^{L_p-1} E_p$ is total average channel energy, and $P_W = \mathbb{E}[|s^W[n]|^2] = \sum_{k=0}^{N_{\text{sc}}-1} \mathbb{E}[|X^W[k]|^2]$ is the average transmitted power of the WUS signal.

III. GENERATION FRAMEWORK FOR DFT-S-OFDM-BASED OOK

A generic method to construct LP-WUS subcarrier coefficients $\{X^W[k]\}_{k=0}^{N_{\text{sc}}-1}$ is to use DFT precoding, resulting in a DFT-s-OFDM modulation only for $s^W[n]$ but not for the remaining part of the OFDM signal $s^D[n]$. This is the retained approach by 3GPP [2].

A. DFT-s-OFDM-based OOK

The considered DFT-s-OFDM based OOK generation framework for LP-WUS is schematized in Figure 2.

1) *Input Bits and Manchester Coding*: First, a bit string $b[l] \in \{0, 1\}$, $l = 0, \dots, N_{\text{bit}} - 1$ is taken as input. We will consider that this bit string follows from a Manchester encoding of an original bit string $b_o[n]$, $n = 0, \dots, N_{\text{bo}} - 1$ such that $N_{\text{bo}} = N_{\text{bit}}/2$ and

$$b_o[n] \rightarrow (b[2n], b[2n+1]) = (\overline{b_o[n]}, b_o[n]), \quad (4)$$

where $\overline{b} = (1+b) \bmod 2$ is the NOT (bit-flipping) operation¹.

2) *Bit Spreading*: The bits $b[l]$ are spread by a factor $N_{\text{seg}} = N_{\text{pulse}}/N_{\text{bit}}$ to obtain a sequence of symbols $d[m]$ that will be used to modulate $N_{\text{pulse}} \leq N_{\text{sc}}$ DFT-s-OFDM pulses. If a bit $b[l] = 0$ then it is mapped to an all-zero sequence; otherwise if $b[l] = 1$ it is mapped to a (so-called in 3GPP) overlaid sequence $\tilde{r}_l[n]$, $n = 0, \dots, N_{\text{seg}} - 1$. In general, each bit $b[l]$ can be written as N_{seg} -time repeated as $b_r[m] = b[l_m]$ with $l_m = \lfloor \frac{m}{N_{\text{seg}}} \rfloor$ and element-wise multiplied with a concatenated N_{pulse} -long bit-spreading sequence $r[m] = \tilde{r}_{l_m}[m - N_{\text{seg}} l_m]$. The modulation symbols are thus

$$\begin{aligned} d[m] &= b_r[m] r[m] & \text{for } m = 0, \dots, N_{\text{pulse}} - 1 \\ &= b[l_m] \tilde{r}_{l_m}[m - N_{\text{seg}} l_m]. \end{aligned} \quad (5)$$

3) *DFT-precoding*: The modulation symbols are then DFT-precoded to obtain a set of pre-processed subcarrier coefficients with indexes $0 \leq k \leq N_{\text{pulse}} - 1$ as

$$D[k] = \sum_{m=0}^{N_{\text{pulse}}-1} d[m] e^{-j \frac{2\pi}{N_{\text{pulse}}} km}. \quad (6)$$

4) *FD Post-Processing*: Typical FD processing of DFT-s-OFDM [16] are also considered here. The N_{pulse} coefficients $D[k]$ may be cyclically-extended as well as shaped by an FDSS window before mapping to the N_{sc} WUS subcarriers, such that for $k = 0, \dots, N_{\text{sc}} - 1$,

$$X^W[k] = \eta W[k] D[(k+L) \bmod N_{\text{pulse}}] \quad (7)$$

¹Remark that Manchester coding can also be defined as $(b[2n], b[2n+1]) = (b_o[n], \overline{b_o[n]})$, but (4) corresponds to a more common implementation obtained by XOR of the clock signal and the bit string.

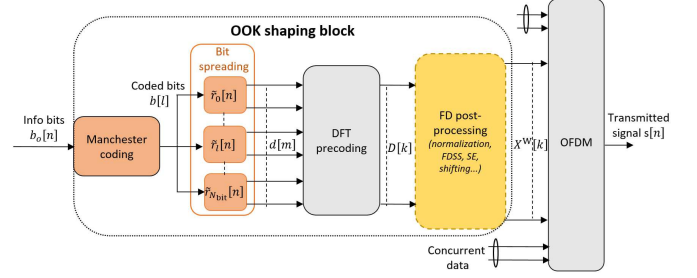


Fig. 2. Illustration of DFT-s-OFDM based OOK modulation

where $(N_{\text{sc}} - N_{\text{pulse}})$ is the spectrum extension (SE), L is an integer shift, $W[k]$ is an FDSS window, and η is a normalization factor.

Conventional DFT-s-OFDM is with $N_{\text{pulse}} = N_{\text{sc}}$, $L = 0$, and then $X^W[k] = \eta D[k]$. SE and FDSS have been considered for low-PAPR (Peak-to-Average Power Ratio) benefit [16], and thus for controlling the envelope of the signal, at the cost of breaking multi-carrier waveform orthogonality and creating ICI. These methods provide similar degrees of freedom in shaping the OOK waveform while for LP-WUS there is no obvious cost in breaking orthogonality.

In addition, SE here enables control of $N_{\text{pulse}} \leq N_{\text{sc}}$ such that the bit spreading factor $N_{\text{seg}} = N_{\text{pulse}}/N_{\text{bit}}$ can be set to be an integer. For example for transmitting $N_{\text{bit}} = 8$ bits in a bandwidth of $N_{\text{sc}} = 12 \times 11 = 132$ then $N_{\text{bit}}/N_{\text{sc}}$ is not an integer; but by selecting $N_{\text{pulse}} = 128$ one is able to satisfy $N_{\text{seg}} = N_{\text{bit}}/N_{\text{pulse}}$ integer.

As for FDSS, we consider possibly complex window but limited to the form $W[k] = e^{-j \frac{12\pi}{N_{\text{fft}}} T_{\text{shift}} k} W_R[k]$ where $W_R[k]$ is a real and symmetric FDSS window and T_{shift} corresponds to a cyclic time shift of the waveform. In this paper we use a Kaiser window, known to concentrate well the energy of DFT-s-OFDM pulses [17], and defined as $W_R[k] = I_0 \left(\beta \sqrt{1 - \frac{(k-\gamma)^2}{\gamma^2}} \right) / I_0(\beta)$ with shaping parameter β and where $\gamma = (N_{\text{sc}} - 1)/2$ and $I_0(\cdot)$ represents the zeroth-order modified Bessel function of the first kind. With $\beta = 0$ $W_R[k] = 1$ for all k i.e. there is no FDSS; and increasing the shaping parameter β increases the FD energy concentration.

The normalization factor η adjust the LP-WUS power. In [2], LP-WUS power spectral density should take into account the guard band usage to be aligned with the concurrent average symbol power P_s , i.e., η in (7) is selected satisfying $\sum_{k=0}^{N_{\text{sc}}-1} \mathbb{E}[|X^W[k]|^2] = P_s(N_{\text{sc}} + N_{\text{GB}})$.

B. TD Pulse Multiplexing Aspect

The inherent TD multiplexing of DFT-s-OFDM makes it suitable for emulating OOK modulation. After inserting (6) and (7) in (2), the WUS can be expressed as

$$s^W[n] = \eta \sum_{m=0}^{N_{\text{pulse}}-1} d[m] g_m[n], \quad (8)$$

which is the multiplexing of symbols $d[m]$ by N_{pulse} pulses

$$g_m[n] = e^{-j \frac{2\pi L}{N_{\text{pulse}}} m} h \left[n - \frac{N_{\text{fft}}}{N_{\text{pulse}}} m \right], \quad (9)$$

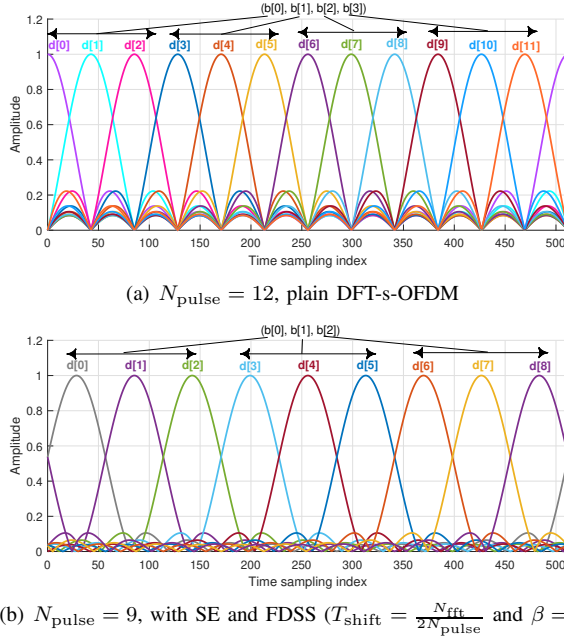


Fig. 3. Illustration of DFT-s-OFDM pulses with $N_{\text{sc}} = 12$. a) 4 bits spread over $N_{\text{pulse}} = 12$ orthogonal plain DFT-s-OFDM pulses. b) 3 bits spread over $N_{\text{pulse}} = 9 \leq N_{\text{sc}}$ non-orthogonal shaped DFT-s-OFDM pulses.

all being time-shifted versions of the same kernel filter

$$h[n] = \sum_{k=0}^{N_{\text{sc}}-1} W[k] e^{j \frac{2\pi k}{N_{\text{fft}}} n}. \quad (10)$$

This filter is the IDFT of the FDSS window. Without FDSS, i.e. all $W[k] = 1$, this reduces to the classical Dirichlet kernel

$$h[n] = e^{j \frac{\pi(N_{\text{sc}}-1)}{N_{\text{fft}}} n} \frac{\sin\left(\pi \frac{N_{\text{sc}}}{N_{\text{fft}}} n\right)}{\sin\left(\pi \frac{1}{N_{\text{fft}}} n\right)}. \quad (11)$$

By inserting (5) in (8), the resulting TD bit multiplexing can be written as

$$s^W[n] = \eta \sum_{p=0}^{N_{\text{bit}}-1} b[p] O_p[n] \quad (12)$$

where $O_p[n] = \sum_{m=pN_{\text{seg}}}^{(p+1)N_{\text{seg}}-1} r[m] g_m[n]$ is the OOK symbol for the p th bit. Each pulse $g_m[n]$ has most of its energy confined in the sample interval $\left[m \frac{N_{\text{fft}}}{N_{\text{pulse}}}, (m+1) \frac{N_{\text{fft}}}{N_{\text{pulse}}}\right]$ with an energy peak in the middle. Most of the potential combined energy of $O_p[n]$ is thus in the sample interval $\left[\frac{N_{\text{fft}}}{N_{\text{bit}}} p, \dots, \frac{N_{\text{fft}}}{N_{\text{bit}}} (p+1)\right]$. Fig. 3 illustrates this pulse modulation aspect within one OFDM symbol. Remark in Fig. 3(a) that the first pulse is always peaking at time zero with its energy spread equally at the beginning and end of the OFDM symbol. This will result in a circular leakage from the first OOK symbol to the last OOK symbol, but can be attenuated by shifting all pulses to the right using a linear phase in $W[k]$ of $T_{\text{shift}} = \frac{N_{\text{fft}}}{2N_{\text{pulse}}}$ as in Fig. 3(b). Also in Fig. 3(b), SE is applied, which decreases the number of pulses and spread them apart; and the pulse kernel (10) is shaped with $\beta = 2$ which has the typically effect to enlarge its main lobe while attenuating its sidelobes. As a result of both SE and FDSS the pulses are non-orthogonal.

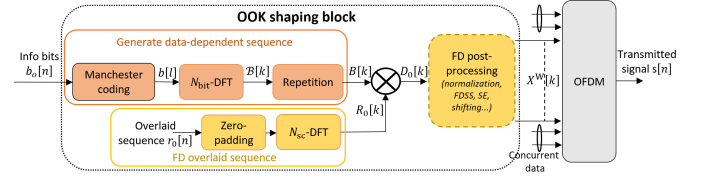


Fig. 4. Equivalent FD implementation of DFT-s-OFDM based OOK in Fig. 2 when bit-spreading is made of common overlaid sequence $\tilde{r}_l[n] = r_0[n]$.

C. Simplified Subcarrier Coefficients

Consider as bit-spreading a common overlaid sequence $r_0[m]$ possibly covered by linear phase ramp as

$$r[l] = e^{j\Phi l} r_0[m - N_{\text{seg}} l_m]. \quad (13)$$

1) *Two-Layer FD Sequences*: Then, the subcarrier coefficient computation can be simplified as layered FD sequences.

Lemma 1. *With bit-spreading (13), the pre-processed subcarrier coefficients (6) are given by*

$$D[k] = B\left(k - \frac{\Phi N_{\text{pulse}}}{2\pi}\right) R_0\left(k - \frac{\Phi N_{\text{pulse}}}{2\pi}\right) \quad (14)$$

where $B(f) = \sum_{m=0}^{N_{\text{bit}}-1} b[m] e^{-j \frac{2\pi}{N_{\text{bit}}} f m}$ is the interpolated DFT² of the bits; and $R_0(f) = \sum_{l=0}^{N_{\text{seg}}-1} r_0[l] e^{-j \frac{2\pi}{N_{\text{pulse}}} f l}$ interpolated DFT of the overlaid sequence $r_0[n]$

The proof is in Appendix A. Obviously, any cyclic shift L in (7) can be equivalently implemented as a phase ramp with $\Phi = -\frac{2\pi L}{N_{\text{pulse}}}$; but only some phase ramp values can be implemented as a cyclic shift. On one hand, conventional DFT-s-OFDM is with $L = 0$ and a phase ramp offers extra degrees of freedom for signal designs, but on the other hand cyclic shifting may be preferred for implementation specially when it corresponds to well-known operation such as e.g. the so-called ‘fftshift’ with $L = -N_{\text{sc}}/2$; and so we will keep both parameters. More specifically, we have

Corollary 1. *If $\frac{\Phi N_{\text{pulse}}}{2\pi}$ is an integer, then $D[k] = D_0[k - \frac{\Phi N_{\text{pulse}}}{2\pi}]$ is a cyclic-shifted version of*

$$D_0[k] = B[k] R_0[k] \quad (15)$$

where $B[k] = B[k \bmod N_{\text{bit}}]$ is the cyclic extension of the N_{bit} -point DFT of the bits

$$B[k] = \sum_{m=0}^{N_{\text{bit}}-1} b[m] e^{-j \frac{2\pi}{N_{\text{bit}}} k m} \quad (16)$$

and where the FD overlaid sequence $R_0[k] = \sum_{l=0}^{N_{\text{seg}}-1} r_0[l] e^{-j \frac{2\pi}{N_{\text{pulse}}} k l}$ is the N_{pulse} -point DFT of the overlaid sequence $r_0[n]$ with zero padding.

Lem. 1 and Corr. 1 provides a different interpretation of DFT-s-OFDM-based OOK. The sequence R_0 provides a common shaping window, constructing a ON symbol kernel, for all possible data-dependent sequences B . This ON kernel does not depends of the bits values but still depends on the bit number via N_{seg} , setting a proper ON symbol duration. The

²Analogous to the discrete-time Fourier transform (DTFT)

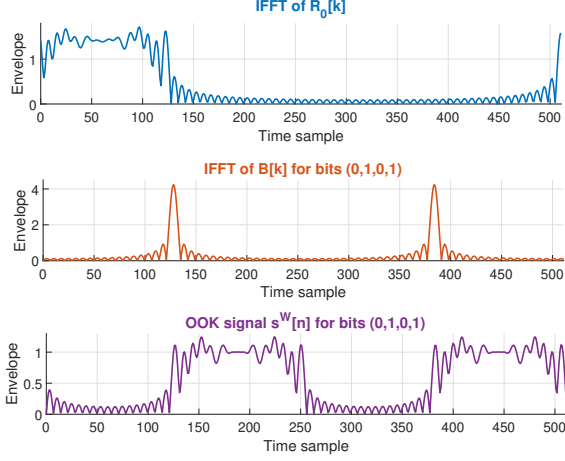


Fig. 5. Illustration of the layered FD sequences B and R_0 .

sequence B carries the bit information by superposing multiple time-shifted version of the same ON symbol kernel. This is illustrated in Fig. 5 for the bit string $(0, 1, 0, 1)$, with $N_{sc} = 72$, a Zadoff-Chu (ZC) sequence as overlaid sequence, and no post-processing. As shown in the figure, the IFFT of $R_0[k]$ creates a single ON symbol while the IFFT of $B[k]$ generates sinc-pulses at different time instants, and the resulting OFDM signal is the convolution of these two signals, up to a scaling.

2) *Implementation Benefits:* In the implementation of Fig. 2, the main complexity lies in the data-dependent N_{sc} -point DFT of Eq. (6). Corr. 1 reveals a lower implementation complexity, as illustrated in Fig. 4: As the sequence $R_0[k]$ is independent of the bits, it can be computed offline and pre-stored. Also due to the repetitive structure of $B[k]$ and since typically $N_{bit} \ll N_{sc}$, computing the N_{bit} -point DFT in Eq. (16) is less complex than computing the DFT in Eq. (6). Moreover, since the input consists of bits, the DFT in Eq. (6) does not actually require any multiplications. For small N_{bit} , which is the regime of LP-WUS in NR, the computation of $B[k]$ can also be made offline and stored in columns of a $N_{bit} \times 2^{N_{bit}}$ look-up table, and $B[k]$ is then directly given by repetitions of $B[k]$ for any bandwidth size N_{sc} .

3) *DFT of the Bits with Manchester Coding:* Furthermore, Manchester encoding can be absorbed in the computation of $B[k]$ to further reduce complexity and storage.

Lemma 2. *With Manchester encoding, the DFT of the encoded-bits $B[k]$, for $k = 0, \dots, 2N_{bo} - 1$, in Eq. (16) can be directly computed from the info bits $b_o[n]$ as*

$$B[k] = \sum_{n=0}^{N_{bo}-1} e^{-j \frac{\pi k}{N_{bo}} (2n + b_o[n])}. \quad (17)$$

The proof in Appendix B. In the case of a small N_{bo} , the values of $B[k]$ can be precomputed and stored in a $2N_{bo} \times 2^{N_{bo}}$ table such that each specific information bit string is mapped to a unique column of this table. Specifically, with $N_{bo} = 1$ and information bit $b_o[0]$, then $B[k]$ reduces to $B[k] = (-1)^{kb_o[0]}$; with $N_{bo} = 2$ and information bits $(b_o[0], b_o[1])$, then $B[k] = (-j)^{kb_o[0]} + (-j)^{k(2+b_o[1])}$. So for $N_{bo} = 1$ or $N_{bo} = 2$, the sequences $B[k]$ are the repetition of the 2 or 4 coefficients of $B[k]$ in Table I.

TABLE I
COEFFICIENTS $B[k]$ FOR MANCHESTER-ENCODING OF ONE OR TWO INFORMATION BITS

$N_{bo} = 1$				
Info bit $b_o[0]$:	0	1		
$\mathcal{B}[0]$	1	1		
$\mathcal{B}[1]$	1	-1		
$N_{bo} = 2$				
Info bit $(b_o[0], b_o[1])$:	(0,0)	(0,1)	(1,0)	(1,1)
$\mathcal{B}[0]$	2	2	2	2
$\mathcal{B}[1]$	0	$1 + j$	$-1 - j$	0
$\mathcal{B}[2]$	2	0	0	-2
$\mathcal{B}[3]$	0	$1 - j$	$-1 + j$	0

IV. RECTANGULAR-LIKE OOK

The intuitive target for designing OOK signals is to create well-formed rectangular waveforms, as initially considered in the 3GPP LP-WUS study [2] using either the LS-precoding method of [14] or a DFT-s-OFDM-based implementation.

A. Flattening ON Symbols in DFT-s-OFDM-based OOK

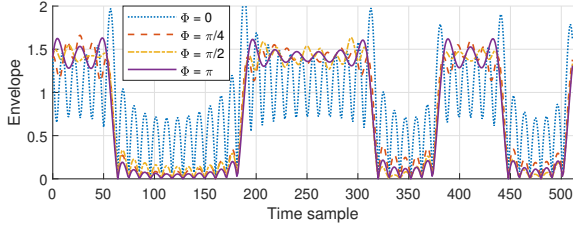
In order to limit envelope fluctuations within ON symbols, one should minimize the phase difference of two crossing neighboring pulses in (12) to control their combining. This resembles low-PAPR methods such as $\pi/2$ -BPSK constellation for DFT-s-OFDM [18]. Following this line of thinking, we consider a linear phase ramp as bit-spreading sequence: $r[m] = e^{j\Phi m}$. Then, as detailed in Appendix C, the coherent combining of two consecutive pulses can be minimized by selecting

$$\Phi = \frac{\pi(2L + N_{sc} - 1)}{N_{pulse}}. \quad (18)$$

This result follows from the analysis of only two overlapping neighboring pulses, and therefore is only an approximation: First, other neighboring pulses also contribute to the envelope fluctuation. Second, if $N_{pulse} \ll N_{sc}$, the neighboring pulses may be so spread apart that their main lobes no longer overlap³. When shaping is applied via FDSS, these discrepancies diminish as the sidelobes are attenuated and the main lobes broaden.

In the case of conventional DFT-s-OFDM with $N_{pulse} = N_{sc}$ and $L = 0$, (18) becomes $\Phi = \frac{\pi(N_{sc}-1)}{N_{sc}} \approx \pi$ and the bit-spreading sequence reduces to a ± 1 alternation as $r[n] \approx (-1)^n$. Fig. 6 shows the effect of the different linear phases $\Phi = 0, \pi/4, \pi/2, \pi$, without and with FDSS. The waveform difference between (18) (exactly here $\Phi = 0.97\pi$) and $\Phi = \pi$ is unnoticeable and thus not shown. Using $\Phi = 0$ results in the worst-case combining for consecutive pulses, leading to significant signal fluctuations and poor OOK signal properties. Without FDSS, a small phase ramp with $\Phi = \pi/4$ already substantially improves the signal shape in both the ON and OFF symbols. With FDSS, a larger phase ramp is needed to further flatten the envelope of ON symbol, albeit at the cost of slower ON/OFF transitions.

³In the case of no FDSS, the main lobe width of the kernel (11) is $2 \frac{N_{fft}}{N_{sc}}$ while pulses are shifted by $\frac{N_{fft}}{N_{pulse}}$ in (9); therefore if $N_{pulse} \leq N_{sc}/2$ the main lobes do not overlap anymore.



(a) Without FDSS

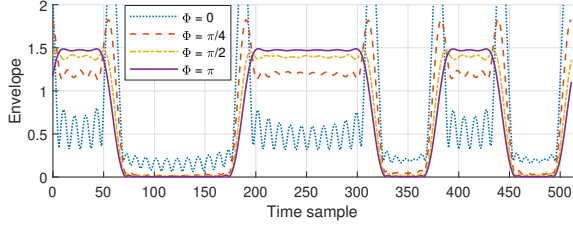
(b) With FDSS ($\beta = 4$)

Fig. 6. OOK waveform flattening effect with increasing angle in linear phase ramp of bit-spreading sequence. Here 8-bit string [10011010] is transmitted with $N_{sc} = N_{pulse} = 48$, and $L = 0$.

With a phase ramp as bit-spreading, the WUS subcarrier coefficients (7) can be further simplified using Lem. 1 and simplifying $R_0(f)$ with the sum exponential formula.

Corollary 2. With $r[m] = e^{j\Phi m}$ for all m , the WUS subcarrier coefficients are given by

$$X^W[k] = \eta W[k] R_0\left(k - \frac{N_{pulse}\Phi}{2\pi} + L\right) B\left(k - \frac{N_{pulse}\Phi}{2\pi} + L\right) \quad (19)$$

where $R_0(0) = N_{pulse}/N_{bit}$ and otherwise

$$R_0(f) = \alpha e^{-j\pi f\left(\frac{1}{N_{bit}} - \frac{1}{N_{pulse}}\right)} \frac{\sin\left(\frac{\pi}{N_{bit}}f\right)}{\sin\left(\frac{\pi}{N_{pulse}}f\right)} \quad (20)$$

in which $\alpha = e^{j\pi\left(\frac{1}{N_{bit}} - \frac{1}{N_{pulse}}\right)\left(\frac{\Phi N_{pulse}}{2\pi} - L\right)}$.

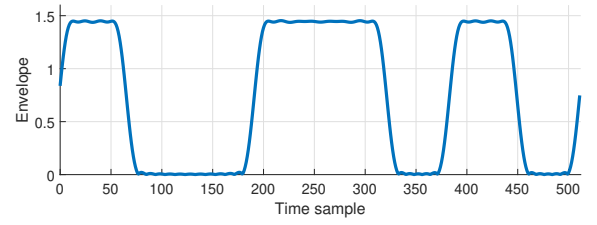
The global phase α has no impact on the signal envelope and can be disregarded.

B. Rectangular Zero-DC OOK

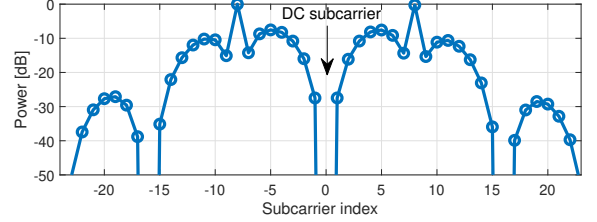
The DC subcarrier is set to zero in the original IEEE 802.11 Wi-Fi signal format to avoid performance degradation due to DC-offset errors. Similarly, the DC subcarrier is nulled in 3GPP LTE standard but not necessarily in NR. A zero-DC OOK was first considered for IEEE 802.11ba WUS [11], [12], [19] but this constraint was eventually relaxed to facilitate the generation of smoother ON/OFF symbols [19], [20].

Using Lem. 1, we observe that this zero-DC constraint can be met if $R_0\left(k - \frac{\Phi N_{pulse}}{2\pi}\right)$ can be nulled at the middle subcarrier index. For rectangular OOK with $R_0(f)$ as given in (20), it is a sinc-like function whose null positions can be controlled by the angle of the phase ramp in the bit-spreading sequence. In general, a null at index k_{null} can be achieved by setting Φ satisfying $R_0(k_{null} - \frac{\Phi N_{pulse}}{2\pi}) = 0$. With $R_0(f)$ in (20), this is achieved by satisfying $\frac{\pi}{N_{bit}}\left(k_{null} - \frac{\Phi N_{pulse}}{2\pi}\right) = \lambda\pi$ with integer $\lambda \neq 0$, giving

$$\Phi = \frac{2\pi}{N_{pulse}}(k_{null} - \lambda N_{bit}). \quad (21)$$



(a) Example of particular signal envelope.



(b) Average power of subcarrier coefficients for Manchester encoded 8-bit string with alternating sign in the ramp phase.

Fig. 7. Illustration of rectangular zero-DC OOK $N_{sc} = 48$ using $\Phi = \pm \frac{2}{3}\pi$.

Assuming $N_{sc} = N_{pulse}$ with DC subcarrier index $k_{null} = N_{sc}/2$, and taking $\lambda = 1$, the DC subcarrier can always be set to zero using $\Phi = \pi\left(1 - \frac{2N_{bit}}{N_{sc}}\right)$. If N_{bit} is small compared to N_{sc} , e.g., $N_{bit} \leq N_{sc}/4$, then as discussed before, Φ would be large enough for the OOK signal to retain a good rectangular shape.

Due to the sinc-like function $R_0(f)$, the power distribution of the subcarriers coefficients will be concentrated in a dominant lobe whose position is also shifted by the phase ramp. To ensure that the LP-WUS average spectrum is symmetrically distributed around the DC, different values of λ can be selected, or the sign of Φ can be alternated in each OFDM symbol. Fig. 7 illustrates the resulting DC nulling effect with $N_{pulse} = N_{sc} = 48$, $N_{bit} = 8$, $k_{null} = 24$, and using $\Phi = \pm \frac{2}{3}\pi$ with alternating sign. As shown, the middle subcarrier has been canceled, while the OOK waveform retains a rectangular shape since $\Phi = \frac{2}{3}\pi$ is close enough to π .

C. Least-Squares (LS) Waveform

In 3GPP LP-WUS study [2] as well as in the on-going 3GPP Ambient-IoT study [21], one of the main approaches is from [14], which provides the LS approximation to an ideal rectangular OOK signal. The subcarrier coefficients are obtained using a so-called ‘‘LS precoding’’ [2], which differs from DFT-precoding in (6). In fact, this method essentially involves a larger DFT of size matching the OFDM IFFT, followed by a truncation to match the bandwidth. See Appendix D for further details.

The LS subcarrier coefficients following [14] can be written for $k = 0, \dots, N_{sc} - 1$ as

$$X^{W,LS}[k] = \eta D^{LS} \left[\left(k - \left\lfloor \frac{N_{sc}}{2} \right\rfloor \right) \bmod N_{fft} \right] \quad (22)$$

where for $l = 0, \dots, N_{fft} - 1$

$$D^{LS}[l] = \sum_{n=0}^{N_{fft}-1} b_s^{LS}[n] e^{-j \frac{2\pi}{N_{fft}} nl} \quad (23)$$

is a N_{fft} -point DFT of the spreaded-bit sequence b_s^{LS} , obtained by repeating the bit string $b[m]$ of length N_{bit} with spreading factor $N_{\text{seg}}^{\text{LS}} = N_{\text{fft}}/N_{\text{bit}}$ (assumed being an integer). Since the perfectly-rectangular OOK signal $b_s^{\text{LS}}[k]$ is real, its spectrum is symmetrically concentrated around the zero frequency. Therefore the LS approximation to $b_s^{\text{LS}}[k]$ with constrained bandwidth is given (22) which preserves the dominant subcarrier coefficients around the zero frequency.

The subcarrier coefficients (22) can be further simplified.

Lemma 3. *The LS coefficients (22) are equivalently given by*

$$X^{W, \text{LS}}[k] = \eta W^{\text{LS}}[k] B \left[k - \left\lfloor \frac{N_{\text{sc}}}{2} \right\rfloor \right] \quad (24)$$

where $W^{\text{LS}}[k] = \frac{N_{\text{fft}}}{N_{\text{bit}}}$ for the middle subcarrier $k = \left\lfloor \frac{N_{\text{sc}}}{2} \right\rfloor$, otherwise for other subcarrier indices $k \neq \left\lfloor \frac{N_{\text{sc}}}{2} \right\rfloor$

$$W^{\text{LS}}[k] = \alpha^{\text{LS}} e^{-j\pi k \left(\frac{1}{N_{\text{bit}}} - \frac{1}{N_{\text{fft}}} \right)} \frac{\sin \left(\frac{\pi}{N_{\text{bit}}} \left(\left\lfloor \frac{N_{\text{sc}}}{2} \right\rfloor - k \right) \right)}{\sin \left(\frac{\pi}{N_{\text{fft}}} \left(\left\lfloor \frac{N_{\text{sc}}}{2} \right\rfloor - k \right) \right)} \quad (25)$$

in which $\alpha^{\text{LS}} = e^{j\pi \left\lfloor \frac{N_{\text{sc}}}{2} \right\rfloor \left(\frac{1}{N_{\text{bit}}} - \frac{1}{N_{\text{fft}}} \right)}$.

The proof is very similar to Lem. 1 and Corr. 2, and therefore is omitted. By identifying with Corr. 2, one derives

Corollary 3. *The LS waveform from (22) can equivalently be generated by DFT-s-OFDM modulation as in (7) with any N_{pulse} satisfying $N_{\text{bit}} \leq N_{\text{pulse}} \leq N_{\text{sc}}$ and $N_{\text{pulse}}/N_{\text{bit}}$ being an integer, if the bit-spreading sequence is a linear phase ramp satisfying $\Phi = \frac{2\pi(L + \left\lfloor \frac{N_{\text{sc}}}{2} \right\rfloor)}{N_{\text{pulse}}}$, and the FDSS window is given for $k \neq \left\lfloor \frac{N_{\text{sc}}}{2} \right\rfloor$ by*

$$W[k] = e^{-j\frac{2\pi k}{N_{\text{fft}}} T_{\text{shift}}} \frac{\alpha^{\text{LS}} \sin \left(\frac{\pi}{N_{\text{pulse}}} \left(\left\lfloor \frac{N_{\text{sc}}}{2} \right\rfloor - k \right) \right)}{\alpha \sin \left(\frac{\pi}{N_{\text{fft}}} \left(\left\lfloor \frac{N_{\text{sc}}}{2} \right\rfloor - k \right) \right)} \quad (26)$$

with $T_{\text{shift}} = \frac{N_{\text{fft}} - N_{\text{pulse}}}{2N_{\text{pulse}}}$, and $W[k] = \frac{N_{\text{fft}}}{N_{\text{pulse}}}$ for $k = \left\lfloor \frac{N_{\text{sc}}}{2} \right\rfloor$.

It is worth noting that for N_{sc} odd, $\left\lfloor \frac{N_{\text{sc}}}{2} \right\rfloor = \frac{N_{\text{sc}}-1}{2}$, and then Φ in Cor. 3 matches exactly (18), which was derived to minimize consecutive pulse combining. For N_{sc} even, these values become approximately equal as N_{sc} increases.

For conventional DFT-s-OFDM with $L = 0$ and $N_{\text{pulse}} = N_{\text{sc}}$, $\Phi = \frac{2\pi}{N_{\text{sc}}} \left\lfloor \frac{N_{\text{sc}}}{2} \right\rfloor$ in Cor. 3, which further simplifies to $\Phi = \pi$ with N_{sc} even. In this case, the LS waveform can be implemented using a ± 1 alternation bit-spreading sequence as $r[n] = (-1)^n$. If one selects $\Phi = 0$ instead, then $L = -\left\lfloor \frac{N_{\text{sc}}}{2} \right\rfloor$, corresponding to the so-called ‘fftshift’ operation that circularly shift the 0th subcarrier coefficient to the middle subcarrier, but applies after repetition if $N_{\text{pulse}} < N_{\text{sc}}$ and not directly after DFT precoding. Intuitively, the LS waveform is obtained by mapping the DC component of the input bit string at the input of DFT precoder to the DC component of the output OFDM signal. An effect of this DC-to-DC mapping is that the LP-WUS signal is a properly interpolated version of the input bits.

The (Φ, L) relationship has an important impact on the signal envelope, and departing too much from it can result in large envelope fluctuation as in Fig. 6. Conversely, the effect

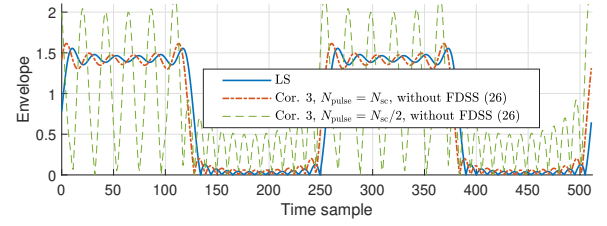


Fig. 8. Illustration of the minor effect of the FDSS window (26) of Cor. 3.

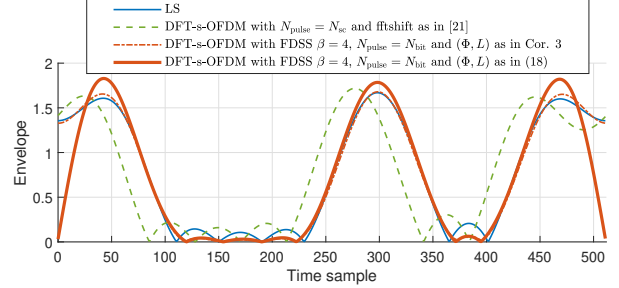


Fig. 9. Example of $N_{\text{bit}} = 6$ bits OOK ([100101]) sent in narrow band of $N_{\text{sc}} = 12$ as considered for Ambient IoT application [21].

of the FDSS window (26) can be negligible especially for $N_{\text{pulse}} = N_{\text{sc}}$ large: When $N_{\text{pulse}} = N_{\text{sc}}$ the amplitude of (26) is nearly constant (almost numerically identical to a Kaiser window with $\beta \approx 2$), and its phase becomes negligible as N_{pulse} grows. Therefore, choosing the largest possible DFT precoder with $N_{\text{pulse}} = N_{\text{sc}}$ may allow the FDSS to be removed with little impact. However when $N_{\text{pulse}} < N_{\text{sc}}$ the FDSS effect becomes more significant. This is illustrated in Fig. 8, which compares the LS waveform obtained from Cor. 3 with and without the FDSS window (26), using $N_{\text{bit}} = 4$ and $N_{\text{sc}} = N_{\text{pulse}} = 48$.

Finally, we remark that in narrowband scenarios such as those in Ambient-IoT applications where larger bit rate and smaller bandwidth than LP-WUS are considered, approximating an ideal –inherently wideband– rectangular signal becomes difficult. In such cases, investigating alternative DFT-s-OFDM-based designs may offer interesting solutions. We provide an example in Fig. 9 for $N_{\text{bit}} = 6$ bits per OFDM symbol using $N_{\text{sc}} = 12$ subcarriers, as considered in [21]. This figure illustrates the DFT-s-OFDM-based implementation therein, corresponding here to $N_{\text{pulse}} = N_{\text{sc}}$, $L = N_{\text{sc}}/2$ (referred as ‘fftshift’), and $\Phi = 0$. This implementation satisfies the relationship between L and Φ as in Cor. 3 but differs from the LS waveform by not including the FDSS (26), which results primarily in a time shifting difference. Fig. 9 also shows an alternative signal design using the minimum number of DFT-s-OFDM pulses $N_{\text{pulse}} = N_{\text{bit}}$ combined with more spectrum shaping using a Kaiser window with $\beta = 4$; and both the (Φ, L) relationship from Cor. 3 and from (18). Since N_{sc} is even and small, we have $\Phi = \pi(L/3 + 2)$ in Cor. 3, which differs from $\Phi = \pi(L/3 + 11/6)$ in (18). As shown, the DFT-s-OFDM waveform with $N_{\text{pulse}} = N_{\text{bit}}$ and Φ from (18) provides better pulse transition and smaller sidelobe in OFF symbols, resulting in power-boosted ON symbols which could facilitate detection.

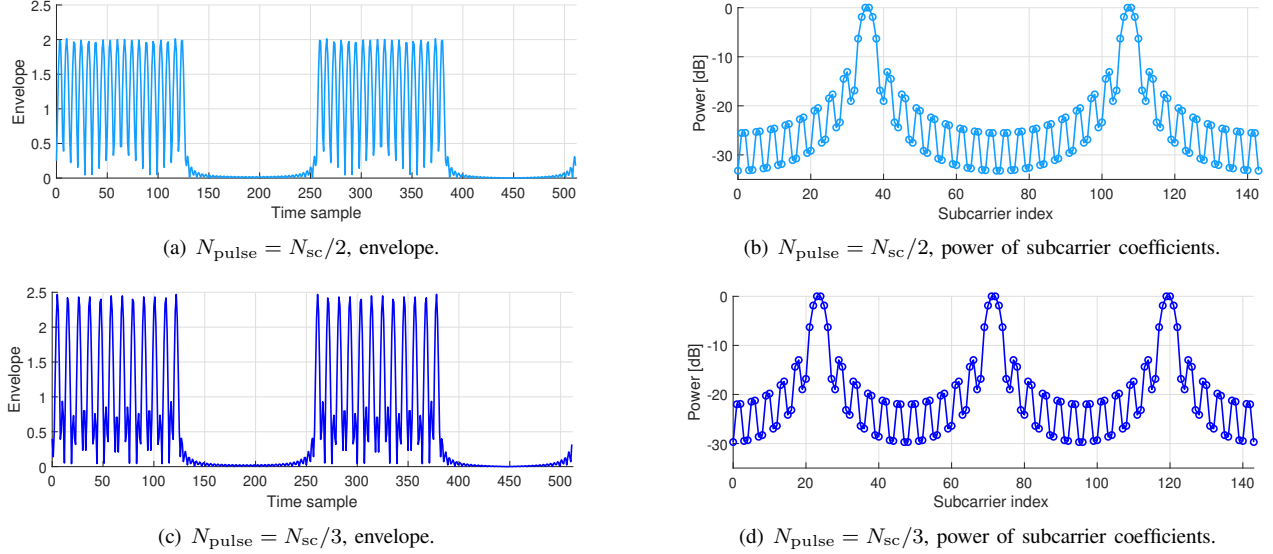


Fig. 10. Illustration of rectangular-like OOK with repeated spectrum using $\Phi = \frac{\pi(2L+N_{\text{pulse}}-1)}{N_{\text{pulse}}}$; with $N_{\text{sc}} = 144$ for bit string [1010].

V. SHAPED OOK FOR 5G LP-WUS

In 3GPP LP-WUS study [2], only $N_{\text{bit}} = 1, 2$, or 4 are considered, while the ADC sampling rate at the LR is assumed to be much higher than such low OOK data rates. Indeed, it was shown therein that an ADC sampling rate of, for example, 3.84 MHz was usable to improve performance while having little impact on the LR's power consumption. With sufficient ADC precision at LR, the OOK detection performance principally depends on the energy split between the ON and OFF symbols, while minimizing the envelope fluctuation inside ON symbols may actually matter little. Therefore, a rectangular-like OOK waveform as targeted in the previous section does not provide the best performance for 5G LP-WUS, and in this section, we discuss two signal features that were recognized in [2] as useful for performance improvement.

A. Spreading OOK Power Spectrum

...for improving performance against frequency-selective fading: An LP-WUS bandwidth no larger than 5 MHz was recommended in [2] to facilitate deployment, amounting to less than 144 subcarriers with 30 kHz spacing in 3GPP numerology. At the same time, larger signal bandwidth can increase frequency diversity and thus robustness against frequency selective fading, such that most sources in [2] considered exploiting as much as possible of this 5 MHz. In this context of a relatively large bandwidth with a low data rate, rectangular-like OOK signals discussed in the previous section have concentrated power spectrum that makes them vulnerable to frequency-selectivity of wireless fading. Alternative signal designs with more spread-out spectrum, but without compromising much on the ON/OFF energy split, can thus improve performance⁴. Below are methods to achieve this.

⁴However, for the purpose of designing OOK synchronization signal, an OOK signal with narrow spectrum can provide benefits for performing frequency-synchronization in frequency-selective channel [22].

1) Frequency-Repetition: Starting from the rectangular-like OOK design discussed so far, a generic method to achieve higher frequency diversity is to repeat its subcarrier coefficients on a wider bandwidth. This can be achieved in (7) by selecting $N_{\text{pulse}} \ll N_{\text{sc}}$, i.e. modulating less, and more spread-apart, DFT-s-OFDM pulses, leading inevitably to a comb-like signal shape. In order to guarantee a good ON/OFF energy split, we first apply (18) to the intermediate narrow band of N_{pulse} subcarriers, i.e. setting $\Phi = \frac{\pi(2L+N_{\text{pulse}}-1)}{N_{\text{pulse}}}$, before repeating in (7) to populate the N_{sc} subcarriers. An example of the obtained waveforms and power distribution over subcarrier indices is shown on Fig. 10 with $N_{\text{sc}} = 144$ and $N_{\text{bit}} = 4$. No FDSS is used here other than a linear phase for time-shifting the signal by half a pulse. As it can be seen the ON symbols cannot be flattened since the main lobes of neighboring pulses simply do not overlap, but by selecting a proper (Φ, L) , the OFF symbols can be guaranteed to be close to zero. Similarly to Fig. 6, variations over (Φ, L) can, in fact, be tolerated with little effect on the signal shape until high envelope lobes are created in the OFF symbols, similar to the green curve of Fig. 8. The drawbacks of such signals are that it may be less robust to lower sampling rate if considered, and may also increase the PAPR of the overall OFDM transmission (depending on concurrent data constellation).

2) Phase Scrambling in Overlaid Sequence: Methods for varying the phase of the overlaid sequence $r_0[k]$ in order to flatten the spectrum were considered in [23]. While by scrambling the phase of the spreading sequence, the envelope shape of the ON symbol may become less controlled, the ON/OFF energy split can still be expected to remain good as it is unlikely that many distant sidelobes in the OFF symbols would coherently combine (cf. $O_p[n]$ in (12) for samples outside of $[pN_{\text{seg}}, (p+1)N_{\text{seg}} - 1]$).

As shown in Corr. 1, the FD power distribution depends on two sequences: $R_0[k]$ from the overlaid sequence, and $B[k]$ from the bits which inherently has a repetition structure such that its power is already well-distributed across the band. We can formalize the following.

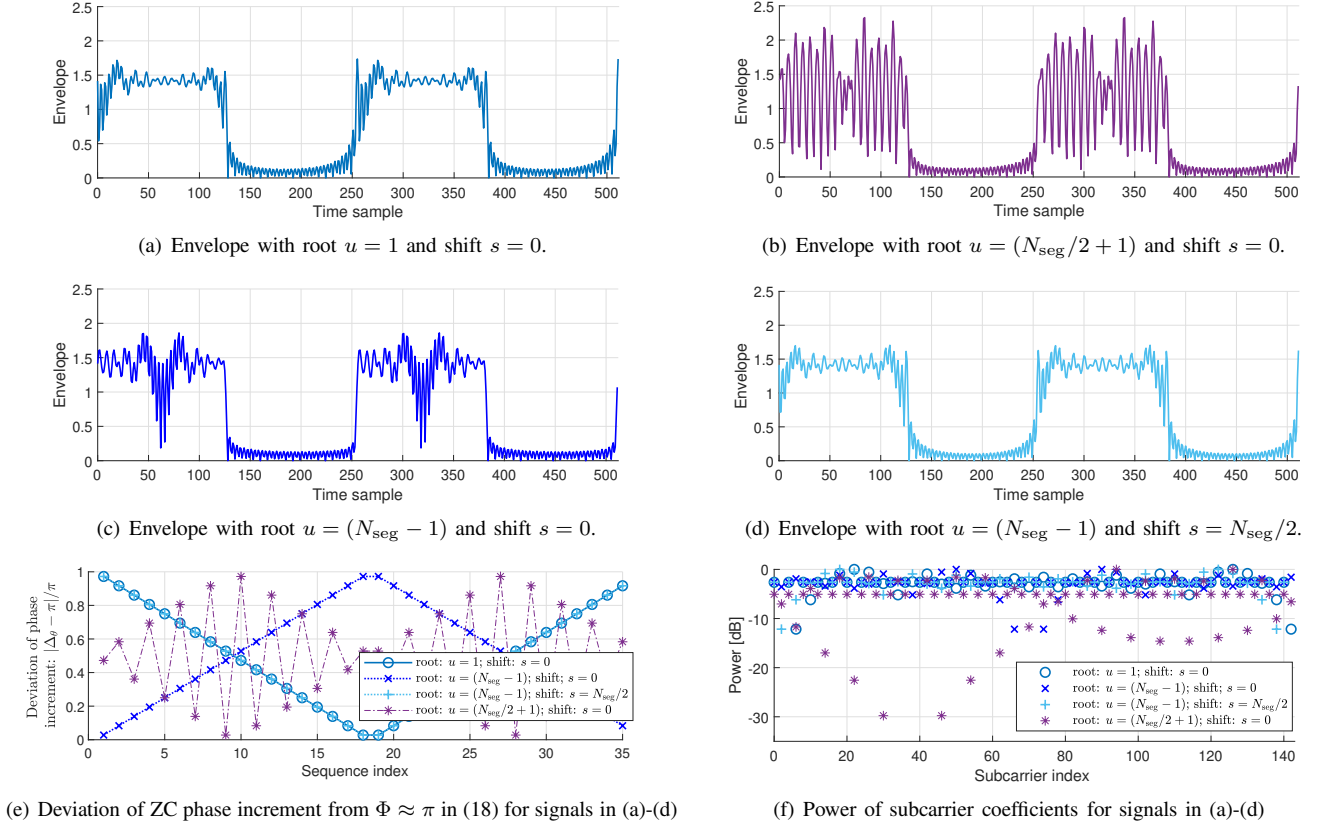


Fig. 11. Examples of OOK signal where $r_0[m]$ is a ZC sequence; $N_{\text{sc}} = 144$ with bit string [1010] and sequence length is $N_{\text{seg}} = 36$.

Lemma 4. *With Manchester coding⁵, half of the total power of $\{D_0[k]\}_{k=0}^{N_{\text{pulse}}-1}$ is always allocated on a comb $\{k = k'N_{\text{bit}}\}_{k'=0}^{N_{\text{seg}}-1}$. On average, the power distribution can be verified to be $E[|D_0[k]|^2] = |R_0[k]|^2 E[|B[k]|^2]$ with*

$$E[|B[k]|^2] = \begin{cases} \frac{N_{\text{bit}}^2}{4} & \text{for } k = (0 \bmod N_{\text{bit}}) \\ \frac{N_{\text{bit}}}{4} \left(1 - \cos \frac{2\pi k}{N_{\text{bit}}}\right) & \text{otherwise} \end{cases} \quad (27)$$

While having half of the power distributed on this comb is independent of $R_0[k]$, the power level fluctuation on it depends on $R_0[k]$. More precisely, $R_0[k]$ is an interpolation of the DFT of $r_0[l]$, $R'_0[k] = \sum_{l=0}^{N_{\text{seg}}-1} r_0[l] e^{-j\frac{2\pi}{N_{\text{pulse}}}kl}$, as

$$R_0[k] = \begin{cases} R'_0[k/N_{\text{bit}}] & \text{for } (k \bmod N_{\text{bit}}) = 0 \\ \frac{1}{N_{\text{seg}}} \sum_{h=0}^{N_{\text{seg}}-1} R'_0[h] I[k - N_{\text{bit}}h] & \text{otherwise} \end{cases} \quad (28)$$

where $I[k] = e^{-j\frac{\pi(N_{\text{seg}}-1)k}{N_{\text{pulse}}}} \frac{\sin(\frac{\pi k}{N_{\text{bit}}})}{\sin(\frac{\pi k}{N_{\text{pulse}}})}$, and the power level on the comb $\{k = k'N_{\text{bit}}\}_{k'=0}^{N_{\text{seg}}-1}$ is completely controlled by the DFT of $r_0[l]$.

a) Random Overlaid Sequence: Randomizing the phase of $r_0[m]$ as considered in [23] would equalize on average the power of its DFT coefficients as $E[|R_0[k]|^2] = N_{\text{seg}}$, which combined with Lem. 4 gives

⁵Without Manchester coding, $E[|B[k]|^2] = \frac{N_{\text{bit}}(N_{\text{bit}}+1)}{4}$ for $k = (0 \bmod N_{\text{bit}})$ and $E[|B[k]|^2] = \frac{N_{\text{bit}}}{4}$ otherwise; and more than half, precisely $\frac{(N_{\text{bit}}+1)}{N_{\text{bit}}}$, of the total average power is allocated on the comb.

Corollary 4. *With random overlaid sequence such that $E[r_0[m]r_0^*[m']] = \delta_{m,m'}$, half of the total average power of $\{D_0[k]\}_{k=0}^{N_{\text{pulse}}-1}$ is equally distributed on a N_{bit} -spaced comb.*

Therefore, this method could ensure a well-spread energy along the band. The drawbacks are that the instantaneous signal is not controlled, and therefore, its knowledge could not be exploited by receivers with higher-end capabilities.

b) Overlaid CAZAC sequence: The approach retained by 3GPP is to use a ZC sequence [23] which is a constant-envelope zero autocorrelation (CAZAC) sequence. A well-known property of a CAZAC sequence is that its DFT is also of constant magnitude [24], such that $|R'_0[h]|^2 = N_{\text{seg}}$ for all h in (28). Combined with Lem. 4 this gives the same result as in Corr. 4 but for each OFDM symbol without averaging.

Corollary 5. *With a CAZAC overlaid sequence, half of the total power of $\{D_0[k]\}_{k=0}^{N_{\text{pulse}}-1}$ is equally distributed on a regular N_{bit} -spaced comb.*

Envelope Shape With Overlaid ZC Sequences: More precisely, if the overlaid sequence is a ZC sequence defined as $r_0[m] = e^{-j\frac{\pi u(m+s)(m+s+\delta)}{N_{\text{seg}}}}$ where $\delta = (N_{\text{seg}} \bmod 2)$, different root $1 \leq u \leq N_{\text{seg}} - 1$ (u must be relative prime to N_{seg}) and shift $0 \leq s \leq N_{\text{seg}} - 1$ would create different ON symbol shapes as shown in Figs. 11(a)-(d) in which $N_{\text{pulse}} = N_{\text{sc}} = 144$, $\Phi = L = 0$, $N_{\text{bit}} = 4$ and $N_{\text{seg}} = 36$. To apprehend this, remark that the phase increment between

consecutive elements in a ZC sequence is a linear function as

$$\Delta_\theta[m] = \angle \frac{r_0[m]}{r_0[m-1]} = -\pi \frac{u(2m+2s-1+\delta)}{N_{\text{seg}}} \mod 2\pi. \quad (29)$$

Comparing to (18) for flattening ON symbols, the closer $\Delta_\theta[m]$ would be constant and close to $\Phi \approx \pi$ in this case, the better the DFT-s-OFDM pulses are expected to constructively combine. The deviations of this linear phase increment Δ_θ from a constant increment of π are shown on Fig. 11(e). With roots closer to $(0 \mod N_{\text{seg}})$, e.g. $u = 1$ or $u = (N_{\text{seg}} - 1)$, the increment changes slower than with ‘middle roots’, e.g. $u = (N_{\text{seg}}/2 + 1)$, which is better for pulse combining. The largest deviations for $(u = 1, s = 0)$ are at the beginning and at the end of the sequence which affect the ON symbol edges. On the contrary, with $(u = N_{\text{seg}} - 1, s = 0)$, the largest deviation is in the middle of the sequence, setting the highest envelope fluctuation right in the middle of the ON symbol. By selecting a different shift $s = N_{\text{seg}}/2$ for $u = (N_{\text{seg}} - 1)$, the deviation of the phase increment then overlaps with case $(u = 1, s = 0)$, and thus both ZC sequences create almost the same OOK envelope shape. Finally, the corresponding powers of subcarrier coefficients for these signals are shown in Fig. 11(f). Every two coefficients are equal to zero which is due to $B[k]$ being equal here to the repetition of the first column in the second table of Table I. Every fourth coefficient has the same power as shown in Corr. 5, accounting for half of the total power as stated in Lem. 4. Other coefficients’ power fluctuates according to (28).

B. Concentrating ON Symbol Energy

...for improving robustness against timing error: It was observed in [2] that while OOK-modulated LP-WUS is robust against frequency synchronization error, it is sensitive to timing error. The larger N_{bit} is, the smaller the OOK symbols are, and the less maximum timing error can be tolerated. LR is expected to use low-cost oscillator with low-precision frequency synchronization, resulting in timing clock drifting. Since LP-WUS is a sporadic message based on needs, its precise transmission time and thus resulting timing drift from previous synchronization acquisition cannot be known at LR. We will model this timing error as uniformly distributed in range $[-\tau_{\text{err}}, \tau_{\text{err}}]$ where τ_{err} is the maximum expected timing error around current receiver timing, given for example from the synchronization signal periodicity.

On Fig. 12, window boundaries for OOK symbol detection are depicted by thick black lines. A normal OOK, where ON symbols have been designed to have their energy spread over one symbol duration as shown in Fig. 12(a), will lead, in case of timing offset at the LR, to a large energy leakage to the adjacent symbol detection window as shown on Fig. 12(b). However, by concentrating the energy of the ON symbols from the right side toward its center as in Fig. 12(c), this energy leakage at the receiver can be significantly reduced as shown on Fig. 12(d), bringing robustness against positive timing offset. Equivalently, concentrating the ON symbol from the left side would bring robustness against negative timing offset.

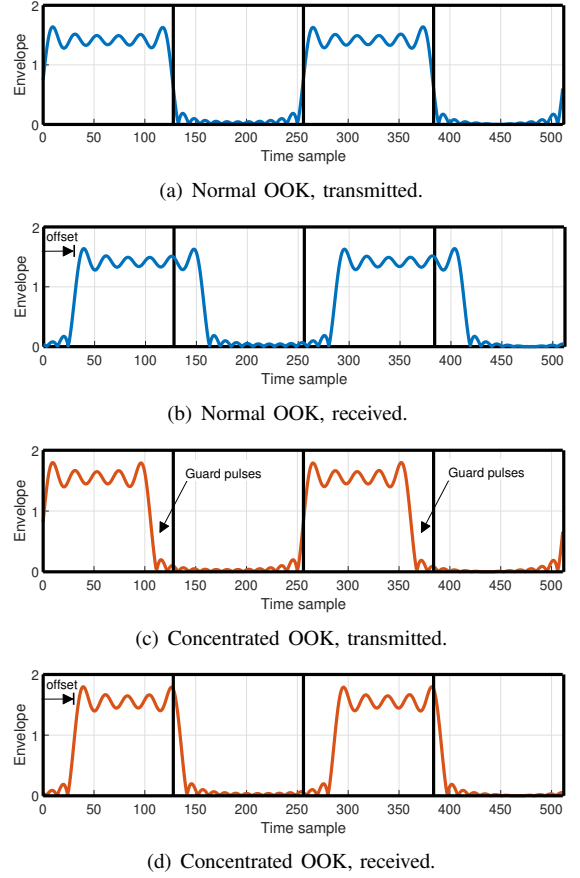


Fig. 12. Illustration of concentrating ON symbol energy against timing error.

Similarly, channel multi-path delays are also likely to cause inter-OOK-symbol interference within one OFDM symbol if there is no guard time between them. Compared to drifting from oscillator which may be assumed to have a symmetrical effect, channel time-dispersion is more likely to result in replica signals with positive delays w.r.t. synchronization timing.

1) *Concentrated DFT-s-OFDM based OOK*: For DFT-s-OFDM based OOK, this energy concentration can be achieved through windowing inside the overlaid sequences $r_0[m]$. To minimize any energy leakage, we consider rectangular windowing by setting the first and last elements in the overlaid sequence $r_0[m]$ to zero. This corresponds to introduce some guard –unmodulated– DFT-s-OFDM pulses in (12). Using N_{Lgp} left and N_{Rgp} right guard pulses, the overlaid sequence satisfies now

$$r_0[m] = 0 \text{ for } \begin{cases} 0 \leq m \leq N_{\text{Lgp}} - 1 \\ N_{\text{seg}} - N_{\text{Rgp}} \leq m \leq N_{\text{seg}} - 1 \end{cases} \quad (30)$$

Obviously, $N_{\text{Lgp}} + N_{\text{Rgp}} < N_{\text{seg}}$ must be fulfilled, and the resulting effective length for using, e.g., a ZC overlaid sequence becomes $N'_{\text{seg}} = N_{\text{seg}} - N_{\text{Lgp}} - N_{\text{Rgp}}$.

2) *How Many Guard Pulses?*: To mitigate also channel time dispersion, it may be beneficial to consider more guard pulses on the right than on the left $N_{\text{Rgp}} \geq N_{\text{Lgp}}$, and thus an asymmetrical ON symbol shape. As one OFDM symbol has a time duration of $1/f_{\text{sc}}$, one pulse has most of its energy spanning a duration of $1/(N_{\text{pulse}}f_{\text{sc}})$. So, in order to cushion

a maximum timing error of τ_{err} in addition to an expected channel spreading of τ_h , a rule of thumb for dimensioning the number of guard pulses is therefore

$$N_{\text{Lgp}} \approx \tau_{\text{err}} N_{\text{pulse}} f_{\text{sc}} \quad (31)$$

$$N_{\text{Rgp}} \approx (\tau_{\text{err}} + \tau_h) N_{\text{pulse}} f_{\text{sc}}. \quad (32)$$

3) *Concentrated Receiver Window*: It is well known from radar literature that a low pulse duty cycle increase peak power, and thus the SNR for a matching receiver integrating then the same signal energy with less noise. This method was proposed in [25] for improving Wi-Fi WUS. However, as pointed in [25], by matching the detection window to the concentrated OOK, the SNR would increase at the cost of an increased sensitivity to timing error. Alternatively, one could also consider to only concentrate the detection window which would in turn improve the robustness against timing error at the cost of a decreased SNR. Hence, for both cases, using a concentrated detection window leads to a trade-off between timing error robustness and SNR. Differently, if only concentrating the transmitted OOK waveform while keeping the original detection window, timing robustness can be improved for the same SNR.

VI. NUMERICAL EVALUATIONS

In this section, the benefits of shaped OOK designs discussed in Section V compared to rectangular OOK designs discussed in Section IV are shown by numerical evaluations in the context of 3GPP simulations assumptions for LP-WUS.

OFDM is configured with $N_{\text{fft}} = 512$, $N_{\text{cp}} = 36$ and $f_{\text{sc}} = 30$ kHz. The total signal bandwidth is 288 subcarriers, of which LP-WUS uses 144 subcarriers inserted in the middle. Out of these, only $N_{\text{sc}} = 132$ are modulated, with guard bands of $N_{\text{GB}} = 6$ subcarriers on each side. Other subcarriers on adjacent channels are modulated by random QPSK symbols. LP-WUS carries $N_{\text{bo}} = 2$ information bits, Manchester-encoded into $N_{\text{bit}} = 4$ bits per OFDM symbol. 3GPP TDL-C channel model is used with 300ns delay scaling and Rayleigh-faded taps according to 3km/h velocity at 2.6 GHz carrier frequency.

At the receiver side, both BPF and LPF are a 3rd order butterworth filter with cutoff bandwidth matching the LP-WUS effective bandwidth of N_{sc} subcarriers. ADC is with a 4-bit quantization precision and a 3.86 MHz sampling rate, corresponding to a downsampled transmitter sampling rate by a factor 4. The LR is assumed to have an automatic gain control, normalizing the received signal envelope by its maximum peak and thus scaling it to the range $[0, 1]$ before quantization. The reference time is assumed to be aligned with first channel tap. Manchester decoding is obtained by segmenting the signal output from the ADC into N_{bit} segments. The sample sums for each pair of segments are then compared for info bit decision.

Fig. 13 shows the bit error rate (BER) for different OOK designs under the assumption of perfect synchronization. The worst-performing curve corresponds to a plain DFT-s-OFDM modulation where bits are only trivially spread using an all-one sequence as $r[m] = 1$, without additional processing (i.e.

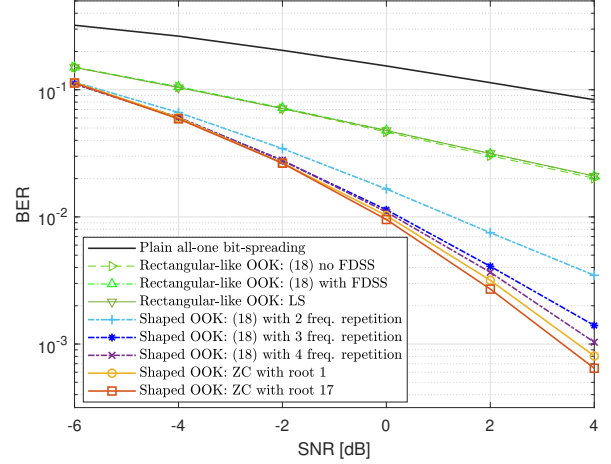


Fig. 13. BER performance comparison between different rectangular OOK designs and shaped-OOK designs with spreaded spectrum.

$L = \Phi = 0$, $N_{\text{sc}} = N_{\text{pulse}}$ and no FDSS as $W[k] = 1$). This method performs poorly because it fails to provide a good energy split between ON and OFF symbols, leading to an envelope shape similar shape to the case of $\Phi = 0$ in Fig.6(a). The rectangular-like OOK signals provide notable detection improvement, as they achieve an excellent energy split between ON and OFF symbols. Three different variations are considered: i) (18) without FDSS; ii) (18) with FDSS using $\beta = 4$ and a time-shifting of half a pulse; and iii) LS waveform discussed in Sec. IV-C. These three rectangular-like OOK designs perform equivalently, showing that envelope fluctuation inside ON symbols has no effect on performance. However, the performance of these designs is limited by their concentrated spectrum. By applying frequency repetition on top of rectangular-like design based on (18) as discussed in Sec. V-A1, the performance improves significantly but saturates after 3 repetitions. Here, 2, 3 and 4 repetitions are achieved by setting $N_{\text{pulse}} = 68, 44$ and 32 , respectively. The best performance is obtained using a ZC overlaid sequence as discussed in Sec. V-A3. In this case, $L = \Phi = 0$, $N_{\text{sc}} = N_{\text{pulse}}$ and there are no FDSS. The length of the ZC sequence is $N_{\text{seg}} = 33$, with two roots, $u = 1$ and 17 , considered. Both roots perform similarly, though the middle root $u = 17$ performs slightly better. This can be attributed to a slightly better ON/OFF energy split with less OFF symbol fluctuation.

In Fig 14, we evaluate the benefit of concentrated OOK for robustness against timing offset (TO). All curves use a ZC overlaid sequence with root $u = 1$ whose length is $N'_{\text{seg}} = N_{\text{seg}} - N_{\text{Lgp}} - N_{\text{Rgp}}$. With $\tau_{\text{err}} = 0$ (i.e. no TO), we found that increasing N_{Rgp} up to $N_{\text{Rgp}} = 6$ can provide a fraction of dB gain. This corresponds to amortizing a channel spreading of $\tau_h = 1.5 \mu\text{s}$, which accounts for absorbing 98% of the average channel energy of the TDL-C channel model. With $\tau_{\text{err}} = 2 \mu\text{s}$ TO, normal OOK experiences a 2dB SNR loss at 10^{-2} BER. Almost all of this performance drop can be recovered by concentrated OOK. Optimization on the number of guard pulses ($N_{\text{Lgp}}, N_{\text{Rgp}}$) to minimize the BER variation at 2dB SNR is shown in the surface subplot at the top right of Fig. 14. It can be seen that the lowest BER (up to simulation precision) is obtained roughly in a zone ($5 \leq N_{\text{Lgp}} \leq 10$, $7 \leq N_{\text{Rgp}} \leq 14$), centered around $(N_{\text{Lgp}}, N_{\text{Rgp}}) = (7, 11)$. This

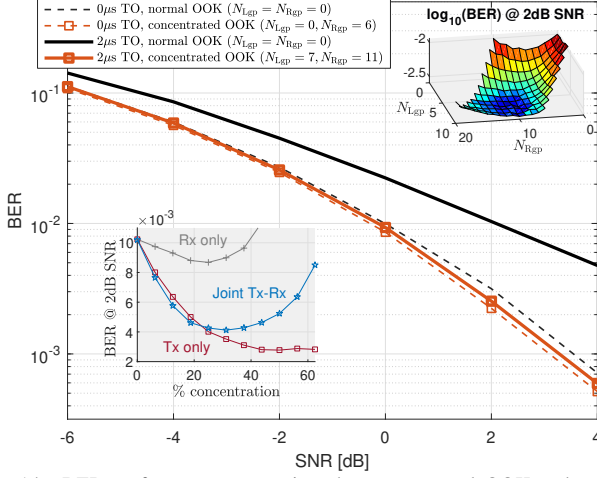


Fig. 14. BER performance comparison between normal OOK and concentrated OOK.

aligns with the anticipation in (31) for compensating the maximum timing offset as here $\tau_{\text{err}} N_{\text{sc}} f_{\text{sc}} = 7.92$. However, the improvement from having an asymmetry $N_{\text{Lgp}} \geq N_{\text{Rgp}}$ shows diminishing returns as N_{Lgp} increases. Moreover, most BER gains can be achieved with fewer guard pulses, e.g. $(N_{\text{Lgp}}, N_{\text{Rgp}}) = (4, 7)$, and additional concentration provides only marginal improvement. When concentration becomes too large, the BER starts to increase as a non-negligible portion of signal energy is lost during receiver downsampling. Finally, in the subplot at the bottom left of Fig. 14, we considered concentrating the Rx detection window by comparing BER at 2dB SNR and $\tau_{\text{err}} = 2 \mu\text{s}$ TO for three cases: i) only the TX signal design is concentrated, ii) only the RX window detection is concentrated, or iii) both are concentrated jointly. For the Tx signal-only concentration, $N_{\text{Lgp}} = N_{\text{Rgp}}$ and the original detection window is used as before, while with joint concentration the detection window is matching the concentrated ON symbol. Concentrating only the Rx detection window provides limited gain. Applying joint concentration offers marginal improvement for small concentration but becomes detrimental with larger concentrations. In these two cases, a trade-off exists between timing error robustness and increased SNR. Ultimately, concentrating only the OOK signal appears to provide the best performance.

VII. CONCLUSIONS

This paper studied a general framework for DFT-s-OFDM based OOK modulation, motivated by the recent adoption of OOK wake-up signals in modern wireless standards. Equivalent frequency-domain implementations were identified. Rectangular-like OOK signals were designed, including with a zero-DC property and equivalent as with the LS precoding method. Finally, shaping methods useful for robustness against frequency-selective fading and timing error were analyzed and numerically evaluated. The results presented herein provide background and further insights into key signal design considerations of 3GPP LP-WUS study. 5G-Advanced LP-WUS OOK signal design, whose details are currently under specification by 3GPP, is expected to be reused for other future IoT technologies such as Ambient-IoT.

APPENDIX

A. General Computation of Subcarrier Coefficients

$$\begin{aligned}
 D[k] &= \sum_{m=0}^{N_{\text{pulse}}-1} b[\lfloor m/N_{\text{seg}} \rfloor] r[m] e^{-j \frac{2\pi}{N_{\text{pulse}}} km} \\
 &= \sum_{m=0}^{N_{\text{bit}}-1} \sum_{l=mN_{\text{seg}}}^{(m+1)N_{\text{seg}}-1} b[\lfloor l/N_{\text{seg}} \rfloor] r[l] e^{-j \frac{2\pi}{N_{\text{pulse}}} kl} \\
 &= \sum_{m=0}^{N_{\text{bit}}-1} b[m] \sum_{l=mN_{\text{seg}}}^{(m+1)N_{\text{seg}}-1} r[l] e^{-j \frac{2\pi}{N_{\text{pulse}}} kl}. \quad (33)
 \end{aligned}$$

Now assuming $r[l] = e^{j\Phi l} r_0[m - N_{\text{seg}} l_m]$, we can apply a change a variable in the inner sum to get

$$\begin{aligned}
 D[k] &= \sum_{m=0}^{N_{\text{bit}}-1} b[m] \sum_{l=0}^{N_{\text{seg}}-1} e^{j\Phi(l+mN_{\text{seg}})} r_0[l] e^{-j \frac{2\pi}{N_{\text{pulse}}} k(l+mN_{\text{seg}})} \\
 &= \sum_{m=0}^{N_{\text{bit}}-1} b[m] e^{j\Phi m N_{\text{seg}}} e^{-j \frac{2\pi}{N_{\text{pulse}}} km N_{\text{seg}}} \sum_{l=0}^{N_{\text{seg}}-1} e^{j\Phi l} r_0[l] e^{-j \frac{2\pi}{N_{\text{pulse}}} kl} \\
 &= \left(\sum_{m=0}^{N_{\text{bit}}-1} b[m] e^{-j \frac{2\pi m (k - \Phi N_{\text{pulse}})}{N_{\text{bit}}}} \right) \sum_{l=0}^{N_{\text{seg}}-1} r_0[l] e^{-j \frac{2\pi l (k - \frac{\Phi N_{\text{pulse}}}{2\pi})}{N_{\text{pulse}}}} \\
 &= R_0 \left[k - \frac{\Phi N_{\text{pulse}}}{2\pi} \right] B \left[k - \frac{\Phi N_{\text{pulse}}}{2\pi} \right] \quad (34)
 \end{aligned}$$

where $R_0[f]$ and $B[f]$ are the interpolated DFT coefficients of the overlaid sequence and the bit sequence, respectively.

B. DFT of Manchester-Coded Bits

By incorporating Manchester coding (4) in the computation of $\mathcal{B}[k]$, (16) becomes

$$\begin{aligned}
 \mathcal{B}[k] &= \sum_{n=0}^{N_{\text{bo}}-1} \overline{b_o[n]} e^{-j 2n \frac{2\pi k}{N_{\text{bit}}}} + b_o[n] e^{-j (2n+1) \frac{2\pi k}{N_{\text{bit}}}} \\
 &= \sum_{n=0}^{N_{\text{bo}}-1} e^{-j 2n \frac{\pi k}{N_{\text{bo}}}} \left(\overline{b_o[n]} + b_o[n] e^{-j \frac{\pi k}{N_{\text{bo}}}} \right) \quad (35)
 \end{aligned}$$

Without loss of generality, we can write

$$\begin{aligned}
 \overline{b_o[n]} + b_o[n] e^{-j \frac{\pi k}{N_{\text{bo}}}} &= \overline{b_o[n]} e^{-j \frac{\pi k}{N_{\text{bo}}} b_o[n]} + b_o[n] e^{-j \frac{\pi k}{N_{\text{bo}}} b_o[n]} \\
 &= e^{-j \frac{\pi k}{N_{\text{bo}}} b_o[n]} (\overline{b_o[n]} + b_o[n]) \\
 &= e^{-j \frac{\pi k}{N_{\text{bo}}} b_o[n]}. \quad (36)
 \end{aligned}$$

and so $\mathcal{B}[k] = \sum_{n=0}^{N_{\text{bo}}-1} e^{-j \frac{\pi k}{N_{\text{bo}}} (2n + b_o[n])}$.

C. Flattening the OOK Waveforms

The phase difference between two neighboring pulses of indices m and $(m+1)$ is

$$\angle \frac{g_{m+1}[n]}{g_m[n]} = -\frac{2\pi L}{N_{\text{pulse}}} + \angle \frac{h \left[n - \frac{N_{\text{fft}}}{N_{\text{pulse}}} (m+1) \right]}{h \left[n - \frac{N_{\text{fft}}}{N_{\text{pulse}}} m \right]}. \quad (37)$$

Then, if the FDSS window is real and symmetric, $W[k] = W_R[k]$, Lem. 1 of [18] gives

$$\angle \frac{h \left[n - \frac{N_{\text{fft}}}{N_{\text{pulse}}}(m+1) \right]}{h \left[n - \frac{N_{\text{fft}}}{N_{\text{pulse}}}m \right]} = -\frac{(N_{\text{sc}} - 1)}{N_{\text{pulse}}} \pi + \theta[n] \quad (38)$$

This can be extended directly to FDSS windows of the form $W[k] = e^{-j\frac{2\pi}{N_{\text{fft}}}T_{\text{shift}}k} W_R[k]$ as such phase shift only changes the overall time position of the pulses.

The function $\theta[n] = \{0 \text{ or } \pi\}$ corresponds to a sign difference between the real part of the pulses, and changes as a function of n . In the case of $N_{\text{pulse}} = N_{\text{sc}}$ and no FDSS, one can verify from (11) $\theta[n] = 0$ for the samples between the two neighboring main lobe peaks, and as N_{pulse} is decreased, $\theta[n] = 0$ in a smaller range of samples around the crossing of the main lobes. Numerical investigation confirms it is also the case with common FDSS windows. So in general $\theta[n] = 0$ where pulse combining should be the most avoided, which leads to

$$\angle \frac{g_{m+1}[n]}{g_m[n]} = -\frac{\pi(2L + N_{\text{sc}} - 1)}{N_{\text{pulse}}} \quad (39)$$

Finally, by selecting $\Phi = \phi_{m+1} - \phi_m = \frac{\pi(2L + N_{\text{sc}} - 1)}{N_{\text{pulse}}}$ we get $\angle \frac{e^{j\phi_{m+1}} g_{m+1}[n]}{e^{j\phi_m} g_m[n]} = 0$.

D. LS Background

In [14], the subcarrier coefficients are obtained as [14, Eq. (8)] $\tilde{\mathbf{x}}_{LS} = (\tilde{\mathbf{F}}^H \tilde{\mathbf{F}})^{-1} \tilde{\mathbf{F}}^H \mathbf{b}_m$ where $\mathbf{b}_m \in \{0, 1\}^{N_{\text{fft}} \times 1}$ contains an upsampled version of the bits string $b[m]$ matching the OFDM IFFT size (i.e. $b_s^L[n]$ in (23)), $\tilde{\mathbf{F}} = \frac{1}{N_{\text{fft}}} [e^{j\frac{2\pi mn}{N_{\text{fft}}}}]_{\substack{n \in \mathcal{K}_c \\ 0 \leq m < N_{\text{fft}}}}$ is a truncated $N_{\text{fft}} \times N_{\text{sc}}$ IDFT matrix whose columns have been restricted to the shifted indexes $\mathcal{K}_c = (\mathcal{K} - k_c) \bmod N_{\text{fft}}$ with $\mathcal{K} = f_0 + \{0, \dots, N_{\text{sc}} - 1\}$ corresponding to the LP-WUS subcarrier allocation and k_c being the center index of the subset \mathcal{K} . The value of the middle subcarrier k_c is not explicitly given in [14], so we will conventionally take $k_c = f_0 + \lfloor \frac{N_{\text{sc}}}{2} \rfloor$ but the alternative $k_c = f_0 + \lceil \frac{N_{\text{sc}}}{2} \rceil$ could also be selected.

In 3GPP study on LP-WUS [2], this construction was discussed as a specific type of precoding, different from DFT, but it is actually simply a DFT where only some outputs are retained. Indeed, the regularization matrix $(\tilde{\mathbf{F}}^H \tilde{\mathbf{F}})^{-1}$ is given following the generic least-squares formulation, however here by construction this simplifies to $(\tilde{\mathbf{F}}^H \tilde{\mathbf{F}})^{-1} = N_{\text{fft}} \mathbf{I}_{N_{\text{sc}}}$ such that this method reduces to $\tilde{\mathbf{x}}_{LS} = \tilde{\mathbf{F}} \mathbf{b}_m$ where $\tilde{\mathbf{F}} = [e^{-j\frac{2\pi mn}{N_{\text{fft}}}}]_{\substack{0 \leq n < N_{\text{fft}} \\ m \in \mathcal{K}_c}}$ is a truncated $N_{\text{sc}} \times N_{\text{fft}}$ DFT matrix where only N_{sc} rows/outputs corresponding of subcarriers indices in \mathcal{K}_c are preserved. Note that the selected DFT output indices \mathcal{K}_c corresponds simply to the baseband subcarrier indices $\mathcal{K}_c = \{-\lfloor \frac{N_{\text{sc}}}{2} \rfloor, \dots, \lfloor \frac{N_{\text{sc}} - 1}{2} \rfloor\} \bmod N_{\text{fft}}$. We encountered in engineer circle that this indexing notation in [14] may be misunderstood by some readers. This is reflected in [6] where the description of [14] is using instead the truncated indices $\{0, \dots, N_{\text{sc}} - 1\}$ which does not correspond to [14] and so the generated LS waveform therein has much less a rectangular shape than the waveform obtained from [14] should have.

E. Proof of Lem. 4

From (15), the average power of the subcarrier coefficients is directly given by $E[|D_0[k]|^2] = |R_0[k]|^2 E[|B[k]|^2]$.

1) *Proof of (27)*: The average $E[|B[k]|^2]$ is derived under the typical assumption of uniformly and independently distributed information bits. As given in Corr. 1, $B[k] = B[k \bmod N_{\text{bit}}]$ has a repetitive structure, so we need only to compute $E[|B[k]|^2]$.

a) *With Manchester coding*: $B[k]$ is given in (17) from Lem. 2. First, it is direct to verify $E[|B[0]|^2] = |B[0]|^2 = N_{\text{bo}}^2$. Then if $k \neq 0$, by expansion we have

$$|B[k]|^2 = N_{\text{bo}} + \sum_{\substack{n, m=0 \\ n \neq m}}^{N_{\text{bo}}-1} e^{-j\frac{2\pi k}{N_{\text{bo}}}(n-m)} e^{-j\frac{\pi k}{N_{\text{bo}}}(b_o[n] - b_o[m])}. \quad (40)$$

Averaging this term above, simplifications are obtained by observing that since $n \neq m$ in the sum the bits are independent, $E[e^{-j\frac{\pi k}{N_{\text{bo}}} b_o[n]}] = \frac{1}{2}(1 + e^{-j\frac{\pi k}{N_{\text{bo}}}})$, and that $|1 + e^{-j\frac{\pi k}{N_{\text{bo}}}}|^2 = 2(1 + \cos \frac{\pi k}{N_{\text{bo}}})$ by expansion and using Euler's formula. Also, we have

$$\begin{aligned} \sum_{\substack{n, m=0 \\ n \neq m}}^{N_{\text{bo}}-1} e^{-j\frac{2\pi k}{N_{\text{bo}}}(n-m)} &= \sum_{n, m=0}^{N_{\text{bo}}-1} e^{-j\frac{2\pi k}{N_{\text{bo}}}(n-m)} - N_{\text{bo}} \\ &= 0 - N_{\text{bo}} = -N_{\text{bo}}. \end{aligned} \quad (41)$$

Putting all that together, we get

$$\begin{aligned} E[|B[k]|^2] &= N_{\text{bo}} + \sum_{\substack{n, m=0 \\ n \neq m}}^{N_{\text{bo}}-1} e^{-j\frac{2\pi k}{N_{\text{bo}}}(n-m)} E[e^{-j\frac{\pi k}{N_{\text{bo}}}(b_o[n] - b_o[m])}] \\ &= N_{\text{bo}} + \frac{1}{2} \left(1 + \cos \frac{\pi k}{N_{\text{bo}}} \right) \sum_{\substack{n, m=0 \\ n \neq m}}^{N_{\text{bo}}-1} e^{-j\frac{2\pi k}{N_{\text{bo}}}(n-m)} \\ &= \frac{N_{\text{bo}}}{2} \left(1 - \cos \frac{\pi k}{N_{\text{bo}}} \right) \end{aligned} \quad (42)$$

which leads to (27).

b) *Without Manchester coding*: To derive the equivalent result without Manchester coding, we average the power of (16) which is $|B[k]|^2 = \sum_{n, m=0}^{N_{\text{bit}}-1} b[n] b[m] e^{-j\frac{2\pi k}{N_{\text{bit}}}(n-m)}$.

For $k = 0$, using the fact that for two independent bits we have $E[b[n]b[m]] = \frac{1}{4}$ and otherwise $E[b[n]^2] = \frac{1}{2}$, we have

$$\begin{aligned} E[|B[k]|^2] &= \frac{N_{\text{bit}}}{2} + \frac{1}{4} \sum_{\substack{n, m=0 \\ n \neq m}}^{N_{\text{bit}}-1} 1 = \frac{N_{\text{bit}}}{4} + \frac{1}{4} \sum_{n, m=0}^{N_{\text{bit}}-1} 1 \\ &= \frac{1}{4} (N_{\text{bit}}^2 + N_{\text{bit}}). \end{aligned} \quad (43)$$

For the case $k \neq 0$, splitting again the case of dependent and independent bits and using a similar identity as (41), we have

$$\begin{aligned} E[|B[k]|^2] &= \frac{N_{\text{bit}}}{2} + \frac{1}{4} \sum_{\substack{n, m=0 \\ n \neq m}}^{N_{\text{bit}}-1} e^{-j\frac{2\pi k}{N_{\text{bit}}}(n-m)} \\ &= \frac{N_{\text{bit}}}{2} - \frac{N_{\text{bit}}}{4} = \frac{N_{\text{bit}}}{4}. \end{aligned} \quad (44)$$

Putting all together, we have

$$E[|B[k]|^2] = \begin{cases} \frac{N_{\text{bit}}(N_{\text{bit}}+1)}{4} & \text{for } k = (0 \bmod N_{\text{bit}}) \\ \frac{N_{\text{bit}}}{4} & \text{otherwise} \end{cases} \quad (45)$$

2) *Half of the Total Power on a Regular Comb*: For a N -length sequence $s = (s[0], \dots, s[N-1])$, let us write its total power as $\|s\|^2 = \sum_{n=0}^{N-1} |s[n]|^2$. The N -DFT is a unitary operation if normalized by $1/\sqrt{N}$, so for the DFT sequence $S[k] = \sum_{n=0}^{N-1} s[n]e^{-j2\pi \frac{nk}{N}}$, its total power is $\|S\|^2 = N\|s\|^2$.

With Manchester coding, the power of the bits string is always $\|b\|^2 = N_{\text{bo}}$, so the total power of the modulating symbols (5) is $\|d\|^2 = N_{\text{bo}}\|r_0\|^2$, and the total power of subcarrier coefficients (6) is $\|D\|^2 = N_{\text{bo}}N_{\text{pulse}}\|r_0\|^2$. Then, the share of power of these subcarrier coefficients on the comb $\{k = k'N_{\text{bit}}\}_{k'=0}^{N_{\text{seg}}-1}$ is

$$\begin{aligned} \sum_{k'=0}^{N_{\text{seg}}-1} |D_0[k'N_{\text{bit}}]|^2 &= \sum_{k'=0}^{N_{\text{seg}}-1} |R_0[k'N_{\text{bit}}]|^2 |B[k'N_{\text{bit}}]|^2 \\ &= N_{\text{bo}}^2 \sum_{h=0}^{N_{\text{seg}}-1} |R'_0[h]|^2 \\ &= N_{\text{bo}}^2 N_{\text{seg}} \|r_0\|^2 \end{aligned} \quad (46)$$

where the second equality follows from (28) and $|B[k'N_{\text{bit}}]|^2 = |B[0]|^2 = N_{\text{bo}}^2$ due to the repetitive structure of $B[k]$. Since $\frac{\sum_{k=0}^{N_{\text{seg}}-1} |D[kN_{\text{bit}}]|^2}{\|D\|^2} = \frac{N_{\text{bo}}N_{\text{seg}}}{N_{\text{pulse}}} = \frac{1}{2}$, half of the total power of the subcarrier coefficients is allocated on this comb.

Without Manchester coding, the *average* total power of the bits string is $E[\|b\|^2] = N_{\text{bit}}/2$, so on average we have also $E[\|d\|^2] = N_{\text{bit}}/2\|r_0\|^2$, and $E[\|D\|^2] = \|r_0\|^2 N_{\text{pulse}} N_{\text{bit}}/2$. The share of average power on the comb is then

$$\sum_{k'=0}^{N_{\text{seg}}-1} E[|D_0[k'N_{\text{bit}}]|^2] = \frac{N_{\text{bit}}(N_{\text{bit}}+1)}{4} N_{\text{seg}} \|r_0\|^2$$

and the ratio is $\frac{\sum_{k=0}^{N_{\text{seg}}-1} E[|D[kN_{\text{bit}}]|^2]}{E[\|D\|^2]} = \frac{(N_{\text{bit}}+1)}{2N_{\text{bit}}} > \frac{1}{2}$.

F. Proof of (28)

By definition $R_0[k] = \sum_{l=0}^{N_{\text{seg}}-1} r_0[l]e^{-j\frac{2\pi kl}{N_{\text{pulse}}}}$. Now assume that the DFT of $r_0[l]$ is $R'_0[h]$ such that $r_0[l] = \frac{1}{N_{\text{seg}}} \sum_{h=0}^{N_{\text{seg}}-1} R'_0[h]e^{j\frac{2\pi lh}{N_{\text{seg}}}}$. Combining them and using the fact that $N_{\text{pulse}} = N_{\text{seg}}N_{\text{bit}}$, we get

$$R_0[k] = \frac{1}{N_{\text{seg}}} \sum_{h=0}^{N_{\text{seg}}-1} R'_0[h] \sum_{l=0}^{N_{\text{seg}}-1} e^{-j\frac{2\pi l(k-N_{\text{bit}}h)}{N_{\text{pulse}}}}. \quad (47)$$

If $k = xN_{\text{bit}}$ with x integer,

$$R_0[xN_{\text{bit}}] = \frac{1}{N_{\text{seg}}} \sum_{h=0}^{N_{\text{seg}}-1} R'_0[h] \sum_{l=0}^{N_{\text{seg}}-1} e^{-j\frac{2\pi l(x-h)}{N_{\text{seg}}}}. \quad (48)$$

The inner sum above is equal to zero if $h \neq x$ and otherwise to N_{seg} , so we have $R_0[xN_{\text{bit}}] = R'_0[x]$ which gives the first line of (28).

If $k \neq xN_{\text{bit}}$, using the sum exponential formula,

$$\sum_{l=0}^{N_{\text{seg}}-1} e^{-j\frac{2\pi l(k-N_{\text{bit}}h)}{N_{\text{pulse}}}} = \frac{\sin\left(\pi \frac{(k-N_{\text{bit}}h)}{N_{\text{bit}}}\right)}{\sin\left(\pi \frac{(k-N_{\text{bit}}h)}{N_{\text{pulse}}}\right)} e^{-j\frac{\pi(N_{\text{seg}}-1)}{N_{\text{pulse}}}(k-N_{\text{bit}}h)} \quad (49)$$

and so we get

$$R_0[k] = \frac{1}{N_{\text{seg}}} \sum_{h=0}^{N_{\text{seg}}-1} R'_0[h] \frac{\sin\left(\pi \frac{(k-N_{\text{bit}}h)}{N_{\text{bit}}}\right)}{\sin\left(\pi \frac{(k-N_{\text{bit}}h)}{N_{\text{pulse}}}\right)} e^{-j\frac{\pi(N_{\text{seg}}-1)}{N_{\text{pulse}}}(k-N_{\text{bit}}h)} \quad (50)$$

which leads to the second line of (28).

REFERENCES

- [1] A. Höglund, M. Mozaffari, Y. Yang, G. Moschetti, K. Kittichokechai, and R. Nory, "3GPP release 18 wake-up receiver: Feature overview and evaluations," *IEEE Commun. Stand. Mag.*, vol. 8, no. 3, pp. 10–16, 2024.
- [2] 3GPP TR 38.869 v1.0.0, "Study on low-power wake up signal and receiver for NR (release 18)," Sep. 2023.
- [3] S. Wagner, K. L. Trung, and R. Knopp, "Low-power wake-up signal design in 3GPP release 18," in *Proc. IEEE Conf. Stand. Commun. and Net.*, 2023, pp. 222–227.
- [4] F. Berggren, A. G. Perotti, and B. M. Popović, "Wake-up signal multiplexing with non-coherently detected waveforms," in *IEEE Veh. Tech. Conf.*, Jun. 2024, pp. 1–6.
- [5] A. G. Perotti, F. Berggren, and B. M. Popović, "Identification codes for wake-up signals," in *Proc. IEEE Int. Conf. Commun.*, Jun. 2024, pp. 3839–3844.
- [6] T. Zhang, M. Afshang, M. Mozaffari, and Y.-P. E. Wang, "Toward zero-energy devices: Waveform design for low-power receivers," *IEEE Commun. Lett.*, vol. 27, no. 8, pp. 2038–2042, 2023.
- [7] T. Zhang, D. Hui, M. Afshang, and M. Mozaffari, "Towards green communication: Soft decoding scheme for OOK signals in zero-energy devices," in *Proc. IEEE Int. Conf. Commun. Workshops*, June 2024, pp. 726–731.
- [8] N. S. Mazloum and O. Edfors, "Performance analysis and energy optimization of wake-up receiver schemes for wireless low-power applications," *IEEE Trans. Wireless Commun.*, vol. 13, no. 12, pp. 7050–7061, 2014.
- [9] 3GPP TSG RAN WG1, "Feature lead summary #3 for 9.4.2.1: Ambient IoT – general aspects of physical layer design," Meeting 117, document R1-2405441, May 2024.
- [10] L. R. Wilhelmsson, M. M. Lopez, S. Mattisson, and T. Nilsson, "Spectrum efficient support of wake-up receivers by using (O)FDMA," in *Proc. IEEE Wireless Commun. Net. Conf.*, 2018, pp. 1–6.
- [11] M. M. Lopez, D. Sundman, and L. R. Wilhelmsson, "Transmitter techniques for multi-carrier on-off keying," in *Proc. IEEE Int. Conf. Commun.*, 2019, pp. 1–6.
- [12] A. Sahin and R. Yang, "Sequence-based OOK for orthogonal multiplexing of wake-up radio signals and OFDM waveforms," in *Proc. IEEE Global Commun. Conf.*, 2018, pp. 1–6.
- [13] A. Sahin, X. Wang, H. Lou, and R. Yang, "Low-PAPR multi-channel OOK waveform for IEEE 802.11ba wake-up radio," in *Proc. IEEE Global Commun. Conf.*, 2019, pp. 1–6.
- [14] N. Mazloum and O. Edfors, "Interference-free OFDM embedding of wake-up signals for low-power wake-up receivers," *IEEE Trans. Green Commun. Networking*, vol. 4, no. 3, pp. 669–677, 2020.
- [15] 3GPP TSG RAN WG1, "Summary #3 of discussions on L1 signal design and procedure for low power WUS," Meeting 112, document R1-2302213, Mars 2023.
- [16] I. P. Nasarre, T. Levanen, K. Pajukoski, A. Lehti, E. Tiirola, and M. Valkama, "Enhanced uplink coverage for 5G NR: Frequency-domain spectral shaping with spectral extension," *IEEE Open J. Commun. Soc.*, vol. 2, pp. 1188–1204, 2021.
- [17] O. Mauritz and B. M. Popovic, "Optimum family of spectrum-shaping functions for PAPR reduction of DFT-spread OFDM signals," in *Proc. IEEE Veh. Tech. Conference*, 2006, pp. 1–5.
- [18] J. Kim, Y. H. Yun, C. Kim, and J. H. Cho, "Minimization of PAPR for DFT-spread ofdm with BPSK symbols," *IEEE Trans. Veh. Tech.*, vol. 67, no. 12, pp. 11 746–11 758, 2018.

- [19] M. C. Caballé, A. C. Augé, E. Lopez-Aguilera, E. Garcia-Villegas, I. Demirkol, and J. P. Aspas, "An alternative to IEEE 802.11ba: Wake-up radio with legacy IEEE 802.11 transmitters," *IEEE Access*, vol. 7, pp. 48 068–48 086, 2019.
- [20] D. S. M. Lopez and L. Wilhelmsson, "MC-OOK Symbol Design," doc. IEEE 802.11-18/0479r2, Mar. 2018.
- [21] 3GPP TSG RAN WG1, "On general aspects of physical layer design for ambient IoT," Meeting 117, document R1-2403954, May 2024.
- [22] —, "Signal design of LP-WUS and LP-SS," Meeting 117, document R1-2403948, May 2024.
- [23] —, "Summary of discussions on L1 signal design and procedure for low power WUS," Meeting 113, document R1-2306234, May 2023.
- [24] B. M. Popović, P. Wang, F. Berggren, and R.-A. Pitaval, "Zero correlation zone sequences with flexible block-repetitive spectral constraints," arXiv:2007.08341, July 2020.
- [25] D. Sundman, M. M. Lopez, and L. R. Wilhelmsson, "Partial on-off keying - a simple means to further improve iot performance," in *Proc. Global Internet of Things Summit*, 2018, pp. 1–5.